Prepared in cooperation with the U. S. Department of Energy, National Nuclear Security Administration, Nevada Site Office, Office of Environmental Management, under Interagency Agreement DE-AI52-01NV13944 Identification and /or Statement of Cooperation

A preliminary investigation of the structure of southern Yucca Flat, Massachusetts Mountain, and CP basin, Nevada Test Site, Nevada, based on geophysical modeling

By Geoffrey A. Phelps, Leigh Justet, Barry C. Moring, and Carter W. Roberts

Open-File Report 2005–1367

U.S. Department of the Interior
U.S. Geological Survey

U.S. Department of the Interior
Gale A. Norton, Secretary

U.S. Geological Survey
P. Patrick Leahy, Acting Director

U.S. Geological Survey, Reston, Virginia 2005

For product and ordering information:
World Wide Web: http://www.usgs.gov/pubprod
Telephone: 1-888-ASK-USGS

For more information on the USGS—the Federal source for science about the Earth, its natural and living resources, natural hazards, and the environment:
World Wide Web: http://www.usgs.gov
Telephone: 1-888-ASK-USGS

A preliminary investigation of the structure of southern Yucca Flat, Massachusetts Mountain, and CP basin, Nevada Test Site, Nevada, based on geophysical modeling

By Geoffrey A. Phelps, Leigh Justet, Barry C. Moring, and Carter W. Roberts

Abstract

New gravity and magnetic data collected in the vicinity of Massachusetts Mountain and CP basin (Nevada Test Site, NV) provides a more complex view of the structural relationships present in the vicinity of CP basin than previous geologic models, helps define the position and extent of structures in southern Yucca Flat and CP basin, and better constrains the configuration of the basement structure separating CP basin and Frenchman Flat. The density and gravity modeling indicates that CP basin is a shallow, oval-shaped basin which trends north-northeast and contains ~800 m of basin-filling rocks and sediment at its deepest point in the northeast. CP basin is separated from the deeper Frenchman Flat basin by a subsurface ridge that may represent a Tertiary erosion surface at the top of the Paleozoic strata. The magnetic modeling indicates that the Cane Spring fault appears to merge with faults in northwest Massachusetts Mountain, rather than cut through to Yucca Flat basin and that the basin is downed-dropped relative to Massachusetts Mountain.

The magnetic modeling indicates volcanic units within Yucca Flat basin are down-dropped on the west and supports the interpretations of Phelps and KcKee (1999). The magnetic data indicate that the only faults that appear to be through-going from Yucca Flat into either Frenchman Flat or CP basin are the faults that bound the CP hogback. In general, the north-trending faults present along the length of Yucca Flat bend, merge, and disappear before reaching CP hogback and Massachusetts Mountain or French Peak.

Introduction

Information regarding groundwater flow paths into and out of Yucca Flat, Nevada Test Site, Nevada, is needed to accurately evaluate the potential for contaminant transport away from Yucca Flat (fig. 1). Groundwater flow through the regional aquifer in the Yucca Flat/CP basin/Frenchman Flat area currently has a high degree of uncertainty. While many tectonic conceptual models for Cenozoic trans-tension in the region suggest that Yucca Flat, CP basin, and Frenchman Flat reside in separate, mechanically unconnected structural domains (e.g., Carr, 1984; Stewart, 1988; and O'Leary, 2000), it is unclear whether the interfaces between the hypothesized tectonic domains promote or hinder lateral groundwater flow through the regional aquifer. This paper presents the results of a new geophysical study that addresses this question.

A preliminary gravity model of Frenchman Flat basin (Phelps and Graham, 2002) indicated that the basin extended into the transition area between Yucca Flat, CP basin,

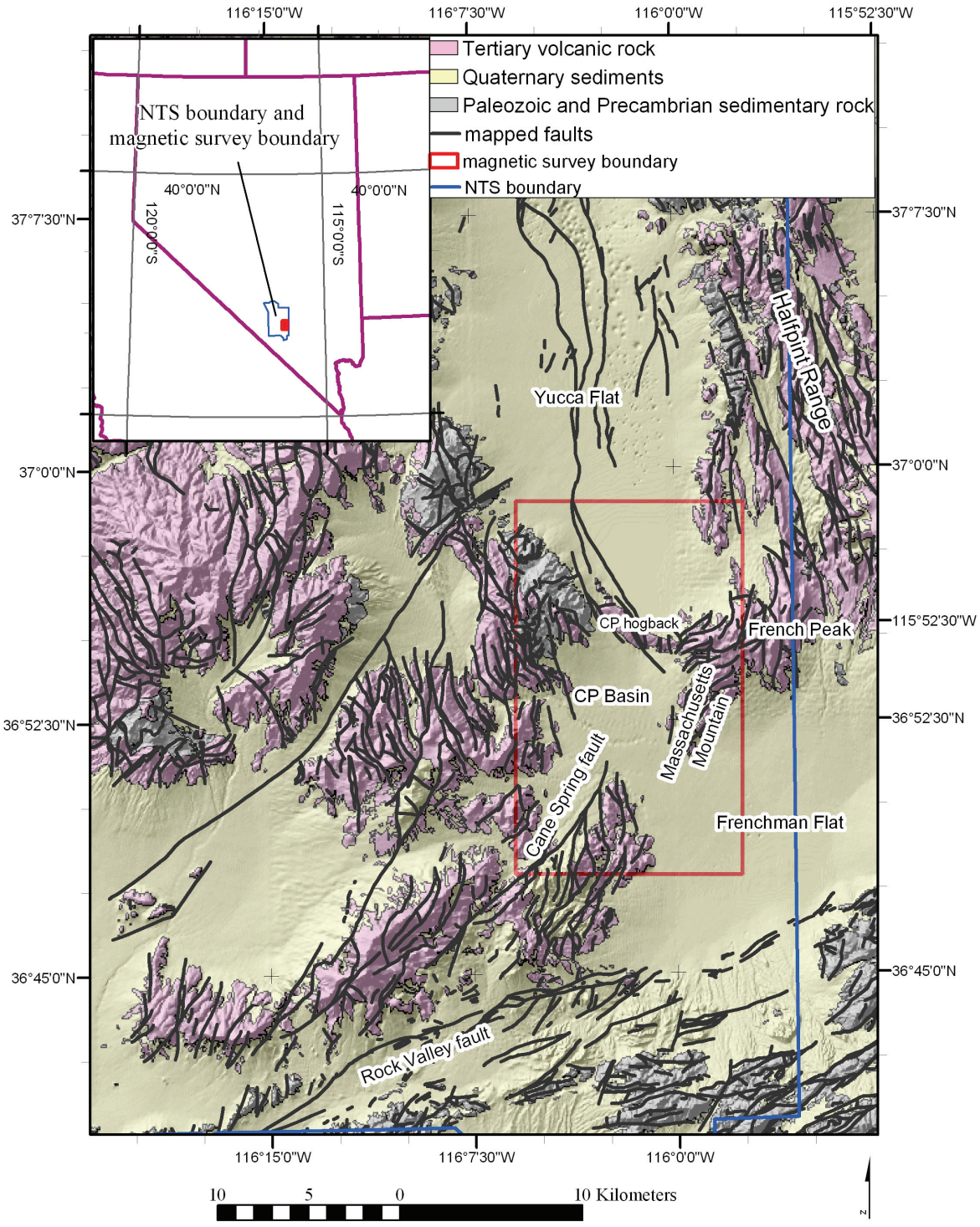

Figure 1. Shaded relief geologic map showing generalized lithologies, faults, and geographic locations mentioned in the text. Geology simplified from Wahl and others (1997), Slate and others (1999), and Raines and others (2003).

and Frenchman Flat, and that Massachusetts Mountain, a topographic high, was underlain by generally lower density basin deposits rather than a pre-Tertiary structural high. Thus previous studies may have placed significant basin-defining structures at least 2 km east of their actual position (e.g. Poole, 1965) and the juxtaposition of the regional aquifer against impermeable Miocene volcanic/volcaniclastic rocks could form a barrier to lateral groundwater flow between CP basin and Frenchman Flat. The available data, however, were insufficient to confirm these conclusions. This study presents the results of a more detailed gravity survey to better understand the Cenozoic structure of the pre-Tertiary rocks in the transitional area between Frenchman Flat and CP basin. These results have implications for the lateral hydrologic connectivity of the regional aquifer between Frenchman Flat and CP basin.

Previous gravity inversion modeling has defined several major north-trending faults in northern Yucca Flat (Phelps and McKee, 1999). The model, however, does not extend southward to CP basin. As a result it is unclear whether north-trending faults in CP basin could juxtapose the regional aquifer against impermeable Miocene volcanic/volcaniclastic rocks and impede lateral groundwater flow between CP basin and Frenchman Flat. This study also presents the results of a high-resolution magnetic survey of the southern Yucca Flat/CP basin/western Frenchman Flat region to confirm the existence and trace the extent of faults in southern Yucca Flat inferred from the previous gravity inversion modeling, and to constrain whether structures in northern CP basin could provide a barrier to lateral groundwater flow from CP basin into Frenchman Flat through the regional aquifer.

Gravity data

Because previous geophysical surveys do not adequately sample Massachusetts Mountain or the area immediately surrounding it, a new high-resolution gravity survey was completed. This more detailed information will better constrain whether or not structurally high basement rocks exist beneath Massachusetts Mountain. CP basin, a potential location for a structural low, was also investigated on its northeast side to examine the structural relationship between Frenchman Flat and CP basin. Data were collected along available roads in the area (fig. 2) and four traverses were completed within the Massachusetts Mountain area between the nearest available roads. In all, data from 143 gravity stations were collected (fig. 2) with a spacing of approximately 300 m along each traverse.

The gravity data were collected using a Lacoste-Romberg gravimeter having a reported precision of 0.001 mGal. Station locations were determined with a Trimble differential real-time kinematic system with a vertical accuracy of 5 to 10 cm. The locational information was used in the final steps of the data reduction process to correct for the distance from the center of the earth (free-air correction) and the effects of topography (complete Bouguer and isostatic corrections).

There are three components to the measurement error: random error (ε), instrument drift (α), and tares (φ). In addition to the instrument's reported precision, the random error includes unpredictable factors such as weather, precision of leveling, temperature, and physical instrument agitation that may occur during a measurement. The error is assumed to follow a Gaussian distribution. Instrument drift is the change, over the time span of a few hours, in the way in which the gravity meter measures gravity. Instrument drift is approximated to a first order by assuming instrument drift changes linearly through time. Tares are a sudden shift in the values recorded by the

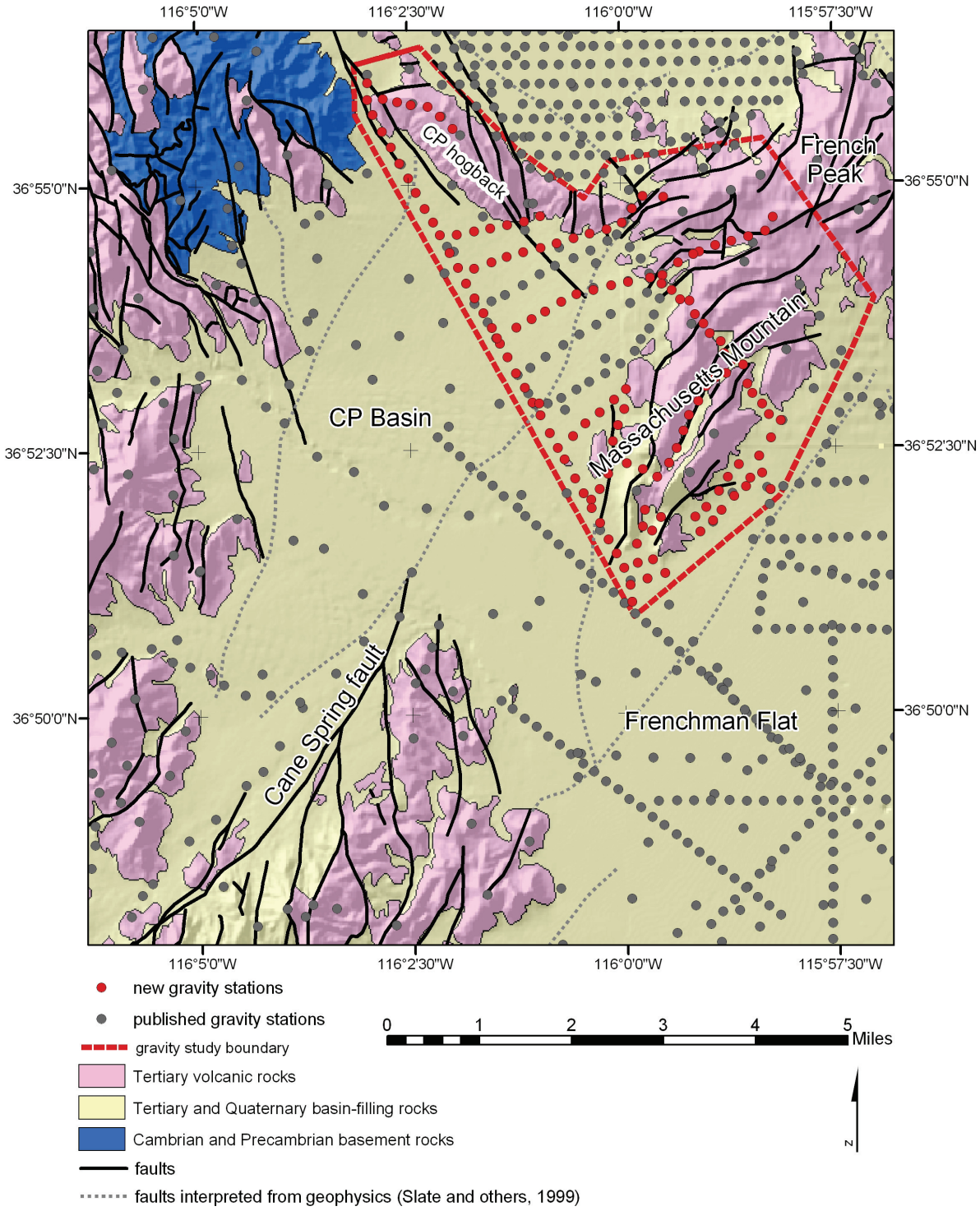

Figure 2. Shaded relief geologic map indicating locations of Tertiary volcanic rocks, Paleozoic and Precambrian basement rocks, basin-filling Quaternary and Tertiary sedimentary rocks, and published and newly collected gravity stations. Geology generalized from Wahl and others (1997) and Slate and others (1999).

instrument. Tares often occur when the instrument is physically jolted. Tares are assumed to occur instantaneously and have a constant value. In addition to the error components, each field measurement is affected by earth tides (Blakely, 1995). The effect of the tides can be calculated and the values are reported in mGal. Repeat measurements were made throughout the survey to monitor for tares in the instrument readings. A tare occurred in the survey on the fifth day.

Because frequent repeat measurements were taken, the following procedure was used to characterize the instrument drift, measurement error, and tare. The observed gravity at a given location can be defined as the gravitational effect measured at a location after all instrument corrections and temporal effects have been applied (equation *1*). This is distinct from other definitions of gravity anomalies (e.g., Bouguer gravity or isostatic gravity anomaly) which additionally correct for spatial effects of elevation and terrain. Equations *1* and *2* $(R_i + \alpha t_i + \varepsilon_i)C_1C_2 + T_i = G_{oi}$ calculate the observed gravity at a given location measured at two different times.

1. $(R_i + \alpha t_i + \varepsilon_i)C_1C_2 + T_i = G_{oi}$

where R_i[1] is the true (unknown) instrument reading at time *i*, without the effects of drift and error, at a given location

α is a constant that accounts for instrument drift as a function of time

t_i is the time of the measurement

ε_i is the measurement error at time *i*

C_1 and C_2 are the manufacturer's correction of 1.021118 and an additional empirical instrument correction of 1.00086 (determined by taking measurements from a range of 53 ft to the top of Mt. Hamilton in Santa Clara County, CA, at 4213 ft), respectively, which convert the measured reading to mGal

T_i is a correction for the influence of the earth tides at time *i*

G_{oi} is the observed gravity at a given location at time *i*

2. $(R_f + \alpha t_f + \varepsilon_f)C_1C_2 + T_f = G_{of}$

where *f* indicates the time of the second measurement.

The equations have two unknowns to solve for, instrument drift, α, and measurement error, ε. The equations can be rearranged to highlight the relationship of the true (unknown) instrument reading, *R*, and the tide correction, *T*.

3a. $(\{R_i + T_i / C_1C_2\}\alpha t_i + \varepsilon_i)C_1C_2 = G_{oi}$

3b. $(\{R_f + T_f / C_1C_2\}\alpha t_f + \varepsilon_f)C_1C_2 = G_{of}$

Without the effects of error or drift, the observed gravity measurements taken at the same location at two different times are equivalent. The $\{R + T/C_1C_2\}$ terms in

[1] The factor $(R_i + \alpha t_i + \varepsilon_i)$ is the measurement seen on the instrument readout, which inherently includes the drift and error components.

equations *3a* and *3b*, therefore, are equal. Assuming no tare has occurred between two measurements taken at the same location and different times, the system of equations can be used to solve for α and ε. Subtracting equation *1* from equation *2* results in equation *4*.

4. $\alpha\Delta t + \varepsilon = \dfrac{\Delta G_o}{C_1 C_2}$

where $\Delta t = t_f - t_i$

ε is the combined error from the two measurements

$\Delta G_o = G_{of} - G_{oi}$

Using equation *4*, a linear model can be fit to a dataset of replicate measurements to solve for the constant α, with Δt as the independent variable, and $\dfrac{\Delta G_o}{C_1 C_2}$ as the dependent variable. If there is a tare, equation 3b becomes

5. $(\varphi + \{R_f + T_f / C_1 C_2\}\alpha t_f + \varepsilon_f) C_1 C_2 = G_{of}$

where φ = tare,

and equation 4 becomes

6. $\varphi + \alpha\Delta t + \varepsilon = \dfrac{\Delta G_o}{C_1 C_2}$

Equation *6* can be solved if there is enough data prior to the occurrence of the tare to obtain an accurate estimate for α using equation *4*. Equation *6* cannot be solved with a linear model because the tare, φ, introduces an abrupt shift in some of the data values. This violates the original assumption that a linear drift, $\alpha\Delta t$, can be applied throughout the entire time of the survey, since the linear model cannot be applied across the tare. If $\alpha = 0$, then equation 5 reduces to

7. $\varphi + \varepsilon = \dfrac{\Delta G_o}{C_1 C_2}$

Equations *4*, *6*, and *7* depend on the change in the observed gravity at a given location, and, therefore, pairs of initial versus final observations can be combined from different locations to collectively analyze the instrument drift.

All locations where repeat measurements were taken were compared by calculating the difference between the measurement at a station and the next measurement in time taken at that location. Dividing these values by the constants C_1 and C_2 yields the dependent variable for equation *4*. All paired measurements that crossed the tare boundary were removed, so that only the drift and measurement error were left uncorrected (see equation *4*). Thirty-nine pairs of measurements were available that did not cross the tare. The data were examined for a linear trend, to see if a linear model could be used to assess the instrument drift. The scatterplot of the data (fig. 3), which has an r^2 value of 0.029, shows that instrument drift does not exhibit a consistent

linear trend over the duration of the survey. The mean of the residuals is close to zero (-0.009), the standard deviation is 0.039, and the distribution of the residuals is approximately Gaussian. Because these conditions are met, the value of the tare can be calculated using equation 7. The mean of all 14 repeat measurements that crossed the tare is taken as the value of the tare. The paired measurements have a mean of 1.400 ± 0.046 (one standard deviation) gravity meter units and tare value of 1.430 mGal. The standard deviation of the error component, based on combining the residuals of both populations and converting the units to mGal, is 0.042 mGal.

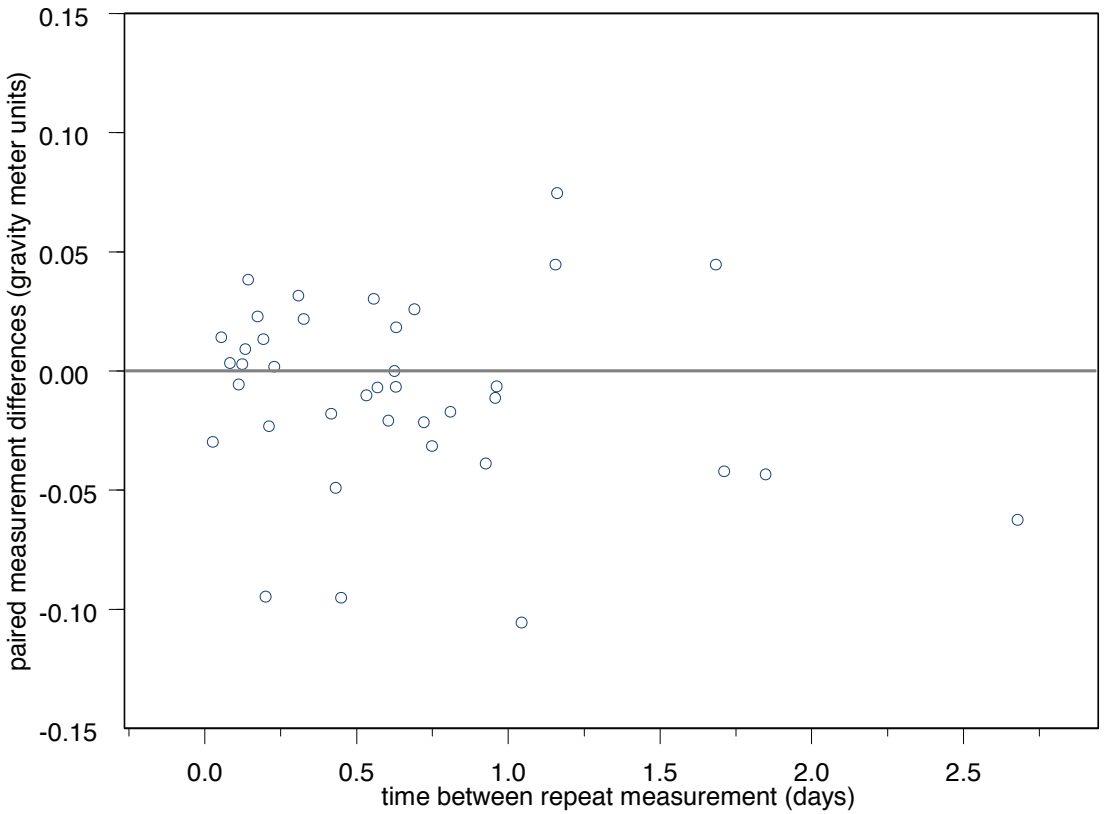

Figure 3. Plot of time between paired measurements and the difference between paired measurements (in gravity meters units), for paired measurements that do not cross the tare.

Once the data were corrected for drift and tare, the reduction process used standard methods outlined by Blakely (1995) to remove the effects of distance from the earth's center of mass, and topography, including the long-wavelength effect from the upper crust (Jachens and Griscom, 1985). Gravity data were reduced using the Geodetic Reference System of 1967 (International Union of Geodesy and Geophysics, 1971) and referenced to the International Gravity Standardization Net 1971 gravity datum (Morelli, 1974, p. 18). Gravity data were reduced to complete Bouguer gravity anomalies (Plouff, 1977) using a reduction density of 2670 kg/m^3 and applying free-air, Bouguer, latitude, curvature, and terrain corrections. An isostatic correction, following the method and parameters used by Jachens and Griscom (1985), was applied to produce the final isostatic gravity anomaly. Assuming a sea level crustal thickness of 25 km, a crustal

density above sea level of 2670 kg/m^3, and a mantle-crust density contrast of 400 kg/m^3, the correction removed the long-wavelength gravitational effect caused by isostatic compensation of topography. The isostatic residual gravity anomaly is the final result of the gravity reduction process. It reflects density variations in the upper 10 km of earth's crust (fig. 4). The data for the gravity survey are contained in appendix A. The newly collected gravity data were combined with existing gravity data for the region (Ponce, 1997) to generate a complete dataset to use for modeling the depth of CP basin.

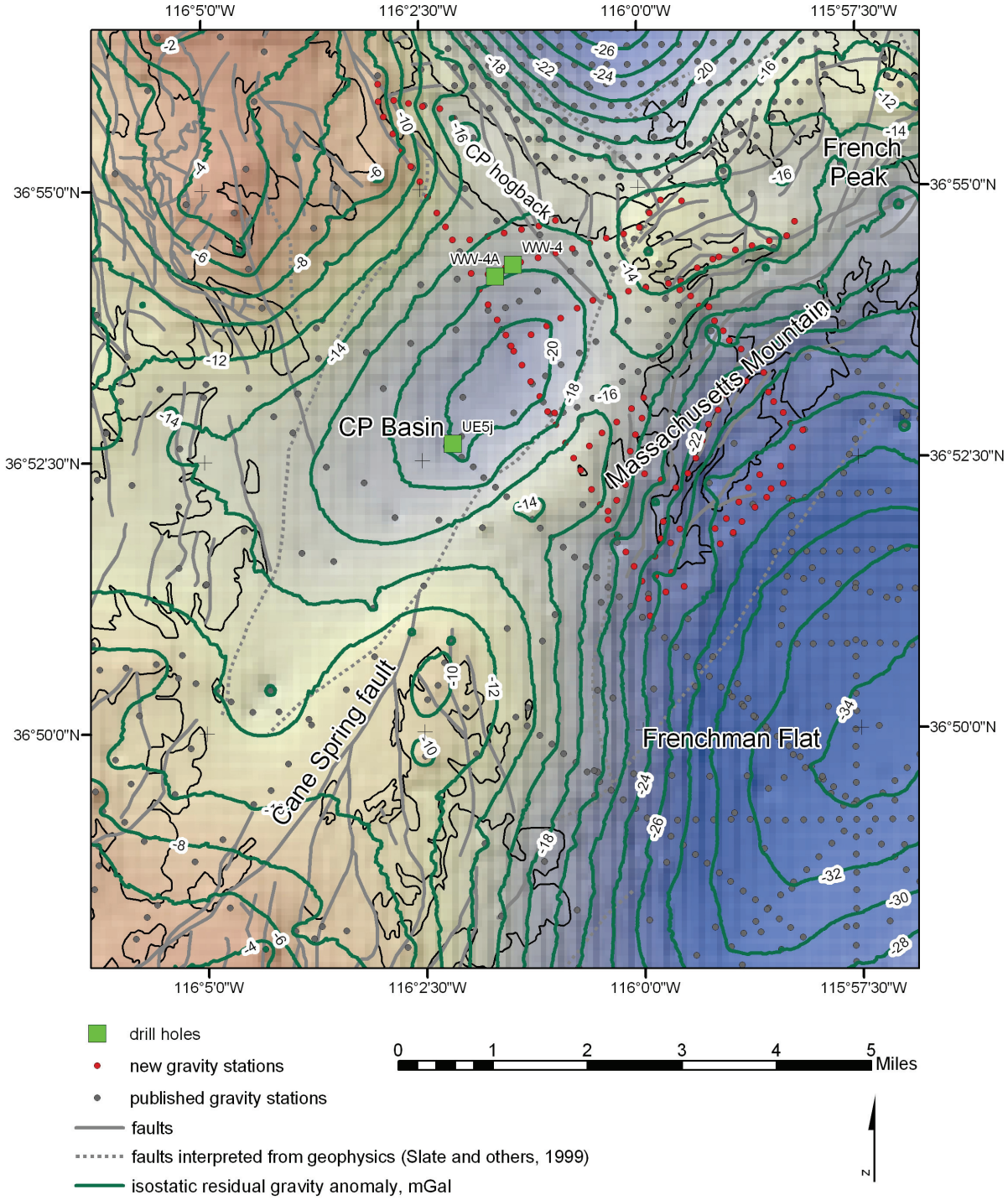

Figure 4. Isostatic residual gravity anomaly shown in shaded relief and with contour lines, using a 2 mGal contour interval. Drill-holes in CP basin shown. Geology generalized from Wahl and others (1997) and Slate and others (1999).

Density data

The isostatic residual gravity anomaly is primarily determined by the densities of mid- to upper-crustal rocks in the nearby region. Characterizing the densities of rocks at the surface and in the subsurface is therefore a central part of the gravity modeling process. By estimating the densities of the rocks, the thickness of rock necessary to produce a given isostatic residual gravity anomaly can be modeled. To estimate the densities of rocks in a given region, surface samples and drill-hole samples and measurements are used. Where drill hole information is available, both lithologic information and drill hole log information, from gamma-gamma density logs and borehole gravity logs, can be used to estimate the change in the density of sediments with depth.

Previous work on the Nevada Test Site has investigated and summarized the rock densities of basin sediments from whole rock samples, gamma-gamma well logs, and borehole gravity well logs (Burkhard, 1989; Phelps and others, 1999; Healey, 1968; Healey and others, 1984; Healey and others, 1986; Kososki and others, 1987; Robbins and others, 1982; Robbins and others, 1983; Schmoker and others, 1978). The most comprehensive study is that of Burkhard (1989), who examined data from 80 drill holes in northern Yucca Flat and described the density distribution for fourteen rock units. Borehole gravity measurements from nine wells within Yucca Flat, three wells within Frenchman Flat, and five wells in the Yucca Mountain area were combined with the drill-hole information on rock units encountered (R. Wahl, written communication) to examine the density distribution of the rock units. Density measurements made using gamma-gamma logs in two recent wells in Frenchman Flat, ER-5-3#2 and ER-5-4#2 (L. Prothro, written communication), were also summarized (fig. 5). The three left-most density data distribution summaries are considered the most reliable because of the larger sample size and the integration of data from multiple locations. The density of the Pre-Tertiary basement rocks is assumed to be 2670 kg/m^3 (average basement density of the Basin and Range, Jachens and Moring, 1990) and is the value used to reduce the gravity data. Previous studies (Phelps and others, 1999) indicate this is a reasonable value for the density of the Pre-Tertiary basement rocks.

Within CP basin, three drill holes penetrate unconsolidated Quaternary sediments, and volcanic rocks from the Ammonia Tanks Formation, Rainier Mesa Formation, and the Paintbrush Group. Density data do not exist for the rocks from these drill-holes; therefore their densities are estimated from the existing density data. The thicknesses of units are not consistent from well to well, indicating the rock units are unevenly distributed within the basin.

Because there is significant variation in possible sediment densities in CP basin (fig. 5), an average density value is used in the models. A lack of density measurements within CP basin, differences in sample sizes of previous studies, and variable thicknesses of the basin-filling rock units within CP basin prevent the use of simple weight average calculations of density. A reasonable density range was chosen for modeling based on the comprehensive study of Burkhard (1989) and the borehole gravity data from Yucca Flat and Yucca Mountain. The range was chosen by using the standard deviation of the data shown in figure 5 that were taken at more than one location. This approach was taken to prevent undue bias from data represented by only a single well (e.g., the three wells in Frenchman Flat). Note that this range also includes the mean values for most of the other data sets. The central value of the range is 1940 kg/m^3, and was chosen as the

preferred value to use for the modeling. The end-member values of the range, 1520 kg/m^3 and 2360 kg/m^3, were used to set reasonable bounds on the uncertainty of the model. Without density data from within CP basin, it is difficult to constrain the density model further.]

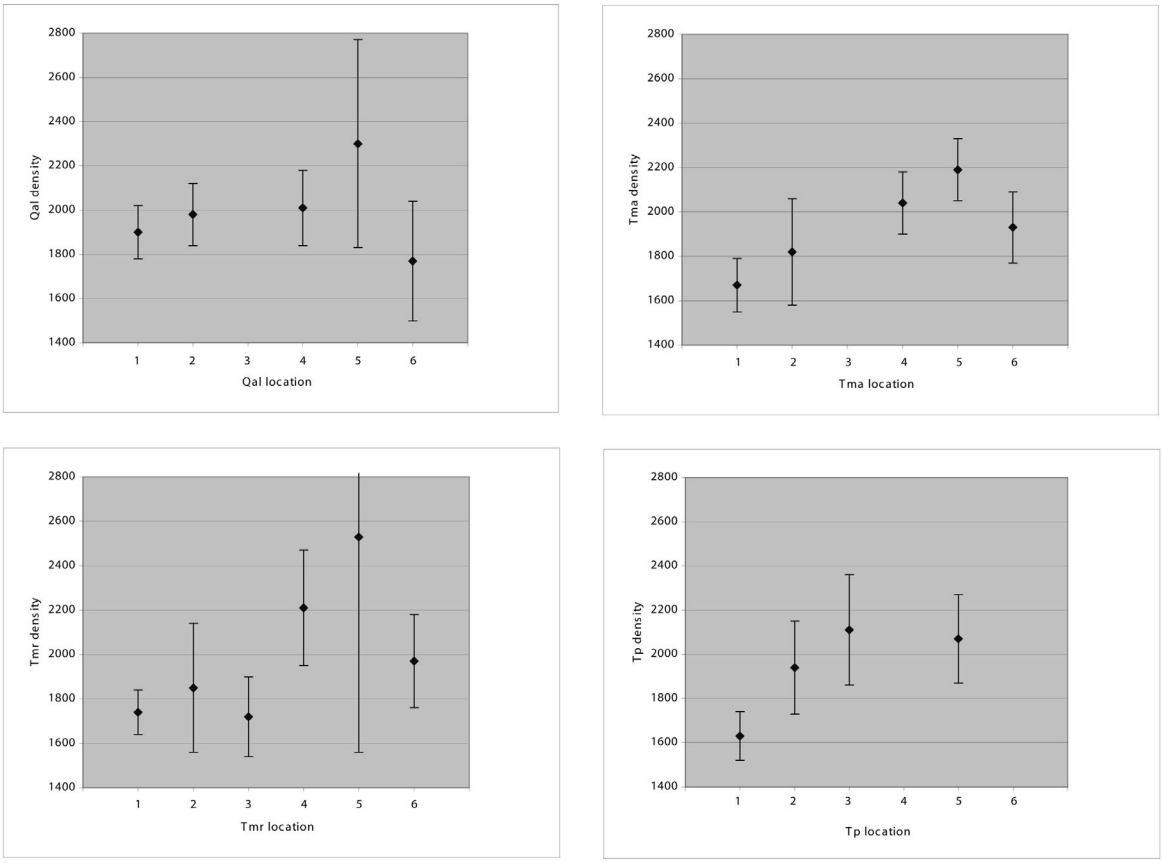

Figure 5. Average densities and the corresponding standard deviations for the four rock units encountered in the wells in CP Basin. 1 is the summarized data from Burkhard (1989), 2 summarizes borehole gravity data from Yucca Flat, 3 summarizes borehole gravity data from Yucca Mountain, 4 summarizes borehole gravity data from Frenchman Flat, 5 is the average values from well ER-5-3#2 from Frenchman Flat, and 6 is the average values from well ER-5-4#2 in Frenchman Flat.

Method

Three estimates of density were used to create three models of the depth to pre-Tertiary basement rocks beneath Massachusetts Mountain and CP basin. The intermediate density value is used to generate the preferred model, while the two bracketing density values are used to generate models that estimate the range of possible solutions and to estimate the uncertainty of the depth predicted by the preferred model.

Modeling the depth to the pre-Tertiary basement depends on the density contrast between basement rock and basin fill. A method developed by Jachens and Moring (1990) separates the observed gravity into two components, dense basement rock-derived and less dense overlying basin-filling deposit-derived. The basin component is initially estimated from basement rock outcrop data. The basin component is then separated and directly inverted in order to provide an initial estimate of the thickness of the basin deposits. The gravitational effect of the deposits is then calculated and the basement component of the anomaly is adjusted accordingly. The process is repeated until the solution converges.

Local and regional outcrop and regional drill-hole data indicate that the basement is composed of pre-Cenozoic sedimentary rocks. The observed density values of the basement rocks are between 310 and 1150 kg/m^3 higher than the overlying basin-fill deposits. Since the modeling results are sensitive to the density values chosen, drill-hole information is used where possible to constrain local density variations and to provide a check on the estimate of basin thickness. Values chosen for model densities can be adjusted to fit the constraining data derived from drill-holes. In the case of CP basin, no density data is available for the rocks from the three drill-holes present. The total depth of the drill-holes, however, can be used to constrain the minimum depth of the model.

Often the densities of basin-filling rocks are modeled as increasing with depth, because it is assumed that the rocks have been lithostatically compacted in a predictable manner (see, for example, Hildenbrand and others, 1999). However, the variability observed in the change in density of the volcanic rocks with depth shown in the previous section (fig. 5) implies that the variability of the densities of the volcanic rocks in CP basin is larger than the variability of a change in density with depth. Therefore, a single mean density was used for each of the three models. Any model of increasing density with depth using the same constraints falls within the range of the models used.

Results

The modeling indicates that CP basin is a shallow, oval-shaped basin with the major axis trending north-northeast and contains ~800 m of basin-filling volcaniclastic and sediment at its deepest point (fig. 6). The deepest part of the basin is in the northeast while the southern part of the basin is very shallow and implies the presence of only a thin veneer of sediments. CP basin is separated from the deeper, neighboring Frenchman Flat basin by a subsurface ridge. This pre-Tertiary basement structure separates the two basins but is spatially displaced from Massachusetts Mountain, the topographic barrier separating the two basins. The subsurface ridge is sub-parallel to the trend of Massachusetts Mountain, but displaced to the west. This relation may be the result of a Tertiary fluvial erosion surface at the top of the Paleozoic strata which cuts deeper into the Paleozoic strata toward the eastern edge of Massachusetts Mountain (Murray and others, 2001). Concurrently, Miocene volcanic/volcaniclastic rocks may have filled in topographic lows created by erosion in a wedge expected to thicken to the east and south (Hinrichs and McKay, 1965; Murray and others, 2001). Tuffs derived from volcanic centers located further to the west draped over this wedge and filled in topographic lows throughout the Miocene epoch. Subsequent extension-related antithetic faulting in the vicinity of Massachusetts Mountain then may have created the topographically high Massachusetts Mountain observed today (fig. 7).

The gravity model assumes constant density in both the overlying basin-filling rocks and sediments and pre-Tertiary basement rocks. Thus changes in the gravitational anomaly are assumed to be due to changes in basement depth alone. If the actual density differs from the assumed density, the model depth will differ from the actual depth. If the density of the basin-filling rocks and sediments is less than the assumed density, the depth will be shallower than predicted. The opposite is true if the density of the basin-filling rocks and sediments is greater than the assumed density. A change in the predicted depth of the model could be caused by an actual change in the depth of the basin, a change in density of the basement or basin rocks, or a combination of the two.

The three drill-holes in CP basin, WW-4, WW-4A, and UE5j, can be used to check the validity of the depths predicted by the three models (table 1). The shallowest model violates the data at the three drill-holes, because it predicts the basement surface at a shallower depth than the total depth of the drill-holes in all cases. This model is not possible for these areas of CP basin because none of the drill-holes encountered pre-Tertiary basement. It is unlikely that this model is correct in the southern part of the basin, because the large extent of exposed Tertiary Wahmonie formation at the southern end of CP basin (Slate and others, 2000) implies that this formation is also extensive at depth, and the density of the formation (as measured in drill-hole ER-5-4#2), 2170 ± 240 kg/m^3, is similar to the range of density used in the preferred and deeper-bracketing model. It is possible that this model is appropriate in the northern portions of the basin, if the volcanic units at the edges of the basin are anomalously light. This model represents an unlikely, but possible, shallowest depth for the northern part of the basin.

The preferred model and the deeper model are both viable given the drill-hole information. However, volcanic rock outcrops surrounding CP basin indicate that the Wahmonie formation and the tunnel beds are the rocks likely to be present beneath WW-4 and WW-4A, both of which are distal units in this area and therefore would not be expected to be thicker than roughly 100 m (Slate and others, 2000; S. Drellack, written communication). Therefore the preferred model is more consistent with geologic interpretation than the deeper model.

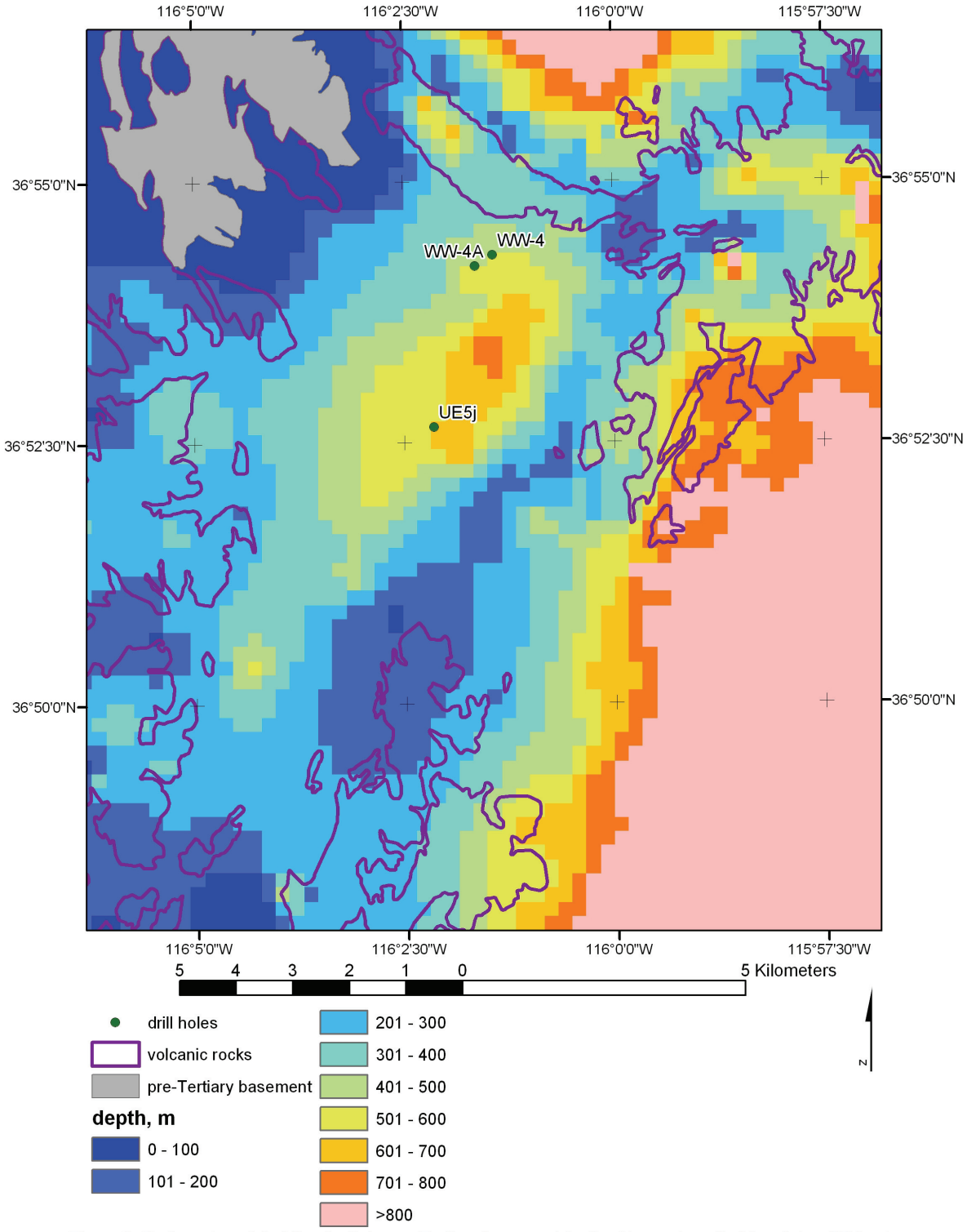

Figure 6. Preferred model of the depth to pre-Tertiary basement for the Massachusetts Mountain - CP basin area. See figure 1b for location information. Geology generalized from Wahl and others (1997) and Slate and others (1999).

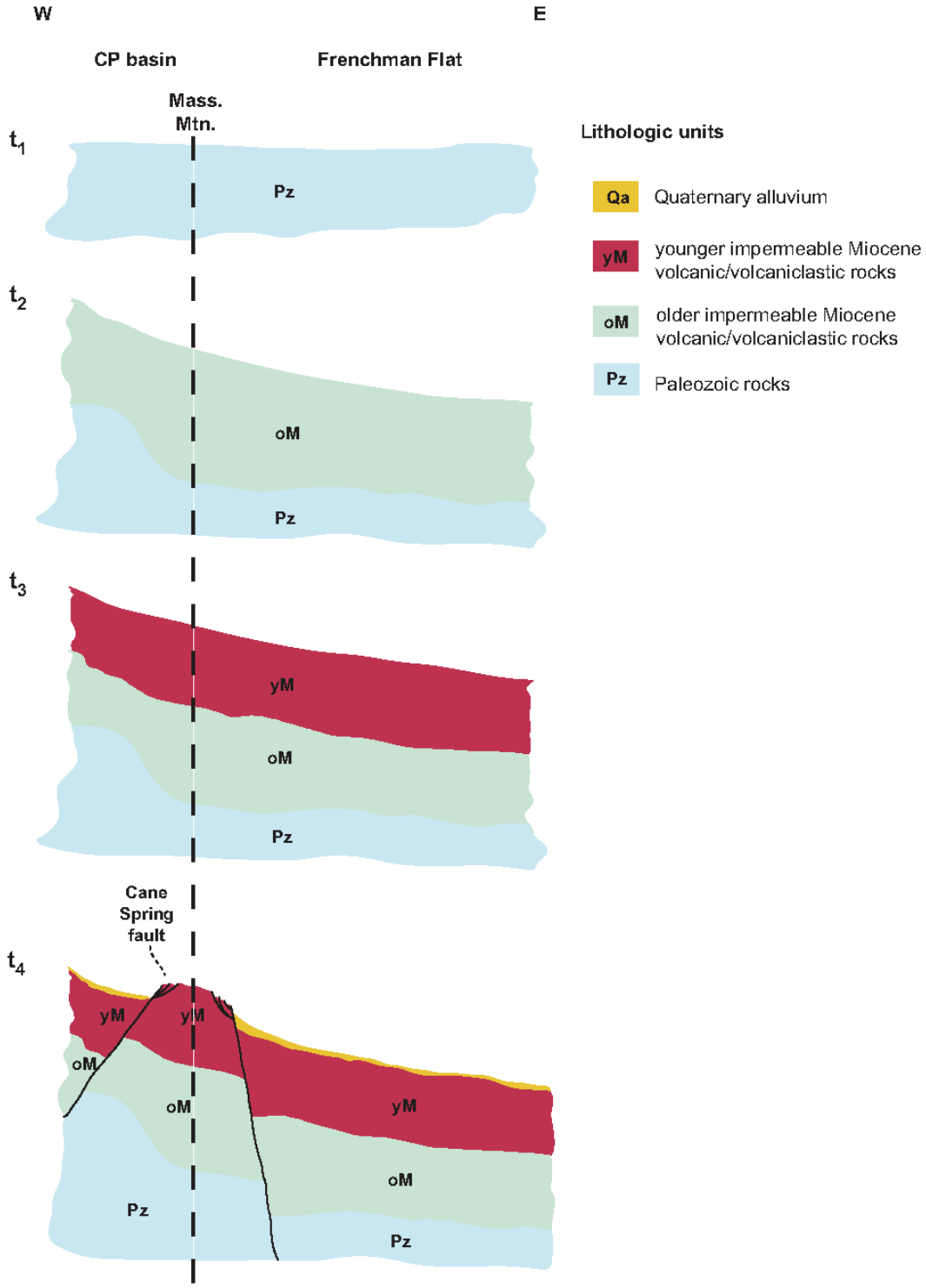

Figure 7. Schematic diagram depicting a possible scenario for the evolution of CP basin and western Frenchman Flat which accounts for the subsurface ridge resolved by density and gravity data. t = time, $t_1 < t_2 < t_3 < t_4$. Not to scale.

drill-hole	total depth	shallow	preferred	deep
WW-4	450.8	291	485	1445
WW-4A	462	295	495	1470
UE5j	378.56	353	609	2091

Table 1. Total depths (meters) of drill-holes in CP basin compare with depths predicted at the drill-hole locations by the three models generated.

Uncertainty

Uncertainty in the data collection stems from several sources, including: measurement error; instrument drift; tide correction error; measurement site location error; and imperfect modeling of topography. The measurement error and instrument drift, discussed previously, were found to be ± 0.042 mGal. The tide correction algorithms produced an error of ±0.001 mGal. To a first approximation, elevation causes a change of a -0.3086 mGal/m of vertical elevation change (Dobrin and Savit, 1988), and the Trimble RTK 4400 GPS instrument used has a vertical accuracy of 5-10 cm. Therefore, with a vertical accuracy of 10 cm, 0.0309 mGal of variation can be expected due to inaccuracies in the measurement of elevation alone. The error due to the Bouguer correction is estimated to be 0.197 mGal/m, and, therefore, 0.020 mGal of variation is contributed by the Bouguer correction. The maximum expected error in the data points after reduction to the complete Bouger anomaly is:

$$\sqrt{(0.042)^2 + (0.001)^2 + (0.0309)^2 + (0.020)^2} = \pm 0.056 \text{ mGal}$$

The uncertainty contributed by the process of interpolating the scattered data points of gravity measurements into a raster isostatic residual anomaly surface is difficult to predict. The gravity data collected in this study was collected at a spacing of roughly 300 m (fig. 2). This resulted in a scattered data set with 50% of the area less than 223 m and 90% of the area less than 600m distance from the nearest data point within the area of the new gravity survey. This can be compared to the scattered dataset for the greater CP basin area, in which 50% of the area is less than 316 m distance from the nearest data point, and 90% of the area is less than 950 m from the nearest data point (fig. 8). The resolution of the new data set is approximately 1.5 times greater than the data set for the greater CP basin area.

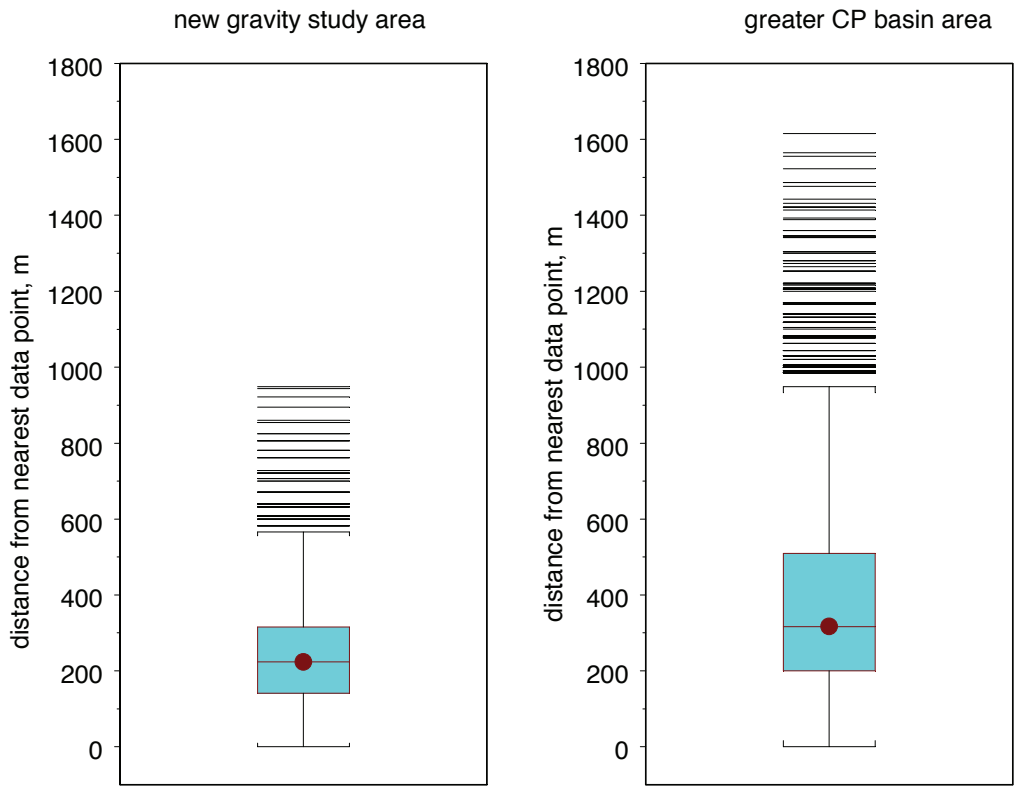

Figure 8. Box plots (Tukey, 1977) showing the distribution of area of the interpolated isostatic residual gravity anomaly that is a given distance from the nearest data point. For the new gravity study area, with more closely spaced gravity measurements (left), 50% of the area is closer than 225 m from the nearest gravity station, comapred to 50% of the area being closer than 310 m from the nearest gravity station for the greater CP basin area (right).

The uncertainty in the gravity modeling can be estimated by examining the range of depths predicted by the range of densities used in this study. The variation within the models is positively correlated with depth. This is a function of the inverse relationship of rock density and predicted depth. As the assumed difference in density between the basement rocks and the basin-filling rocks and sediments decreases, the depth of the basin (that is, the volume of rocks necessary to account for the measured gravity anomaly) increases asymptotically. The range of depth error resulting from an incorrect assumption of density, therefore, will always be greater with greater predicted depth. The range of the model is shown graphically in figure 9. The range of depths among the models can be read directly from the graph. For example, if the preferred model (represented by the horizontal axis) predicts a depth of 600 m, then the less dense model (represented by the orange triangles) predicts a depth roughly 250 m shallower and the densest model predicts a depth roughly 1300 m deeper (both read from the vertical axis of the graph). At shallow depths the difference between the models is minimal. As depth increases the less dense model and the preferred model diverge while the densest model diverges at a much greater rate. The asymmetrical behavior of the uncertainty is characteristic of this type of gravity inversion modeling. The spread among the data points themselves shows that local conditions in the gravity anomaly affect the predicted model depth. This is especially prominent in the deeper model, where small changes in the gravity anomaly have a much larger effect on the predicted depth.

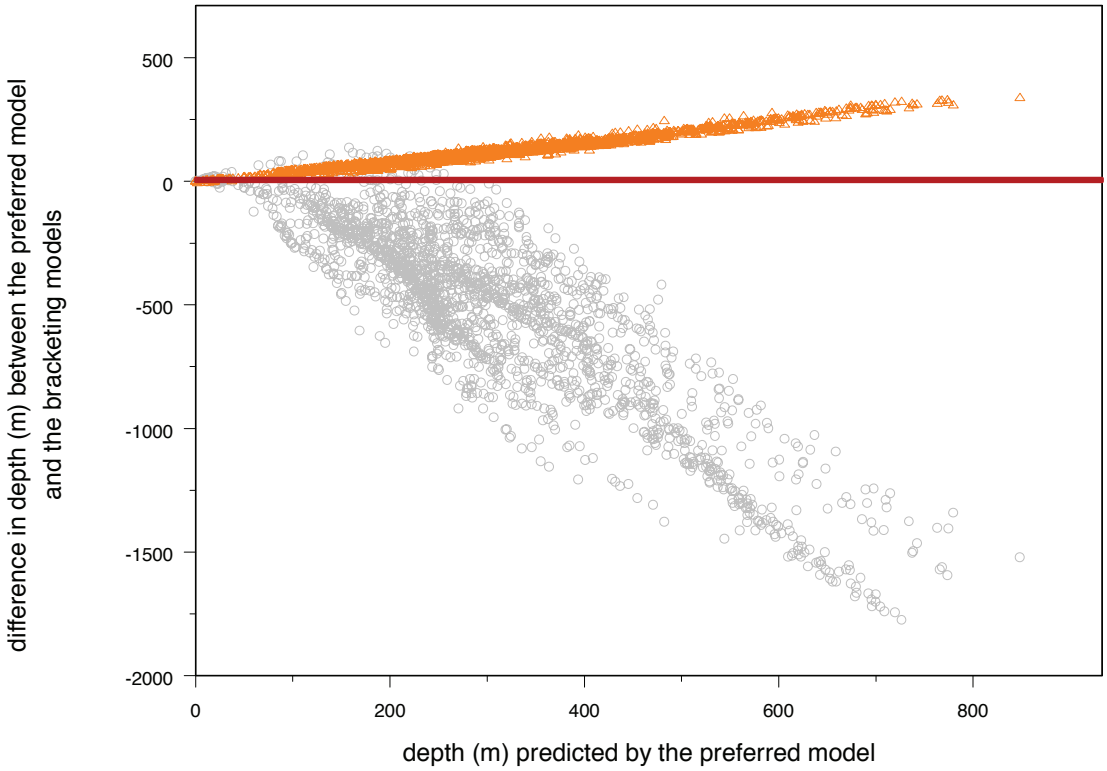

Figure 9. Depth predicted by the preferred model (horizontal axis) compared with depths predicted by the shallower (orange) and deeper (grey) models. As the depth predicted by the preferred model increases, the depths predicted by the bracketing models diverge. The uncertainty increases asymmetrically with depth.

Magnetic data

Gravity modeling indicates that major subsurface north trending faults run the length of the Yucca Flat basin (Healey, 1968; Ferguson and others, 1988; Phelps and others, 1999). Recently, Wahl and others (1997) and Slate and others (2000) proposed that the Cane Spring fault is a basin-crossing structure that extends from the northernmost end to the southern end of CP basin. The prevalence of magnetic tuffs in the southern Yucca Flat/northern CP basin/Massachusetts Mountain area affords an opportunity to use high resolution magnetic data to search for near-surface faults. To this end, we conducted the survey shown in figure 10. The results of this survey will better constrain fault patterns in southern Yucca Flat, CP basin, and the Massachusetts Mountain area.

A high-resolution magnetic survey was flown over the southern Yucca Flat and CP basin area in September, 2003, by a private contractor, Geophex, Ltd. The survey was completed using a helicopter, with a terrain elevation of 122 m and a flight line spacing of 200 m. Flight lines were flown east-west, with north-south tie lines flown every 2 km. The data were corrected by subtracting the base station magnetic data, and remaining leveling errors corrected using tie-line leveling. IGRF2000 was removed from the data, computed using GPS location and elevations at each observation point and the epoch of September 26, 2003. The data were gridded using a minimum curvature

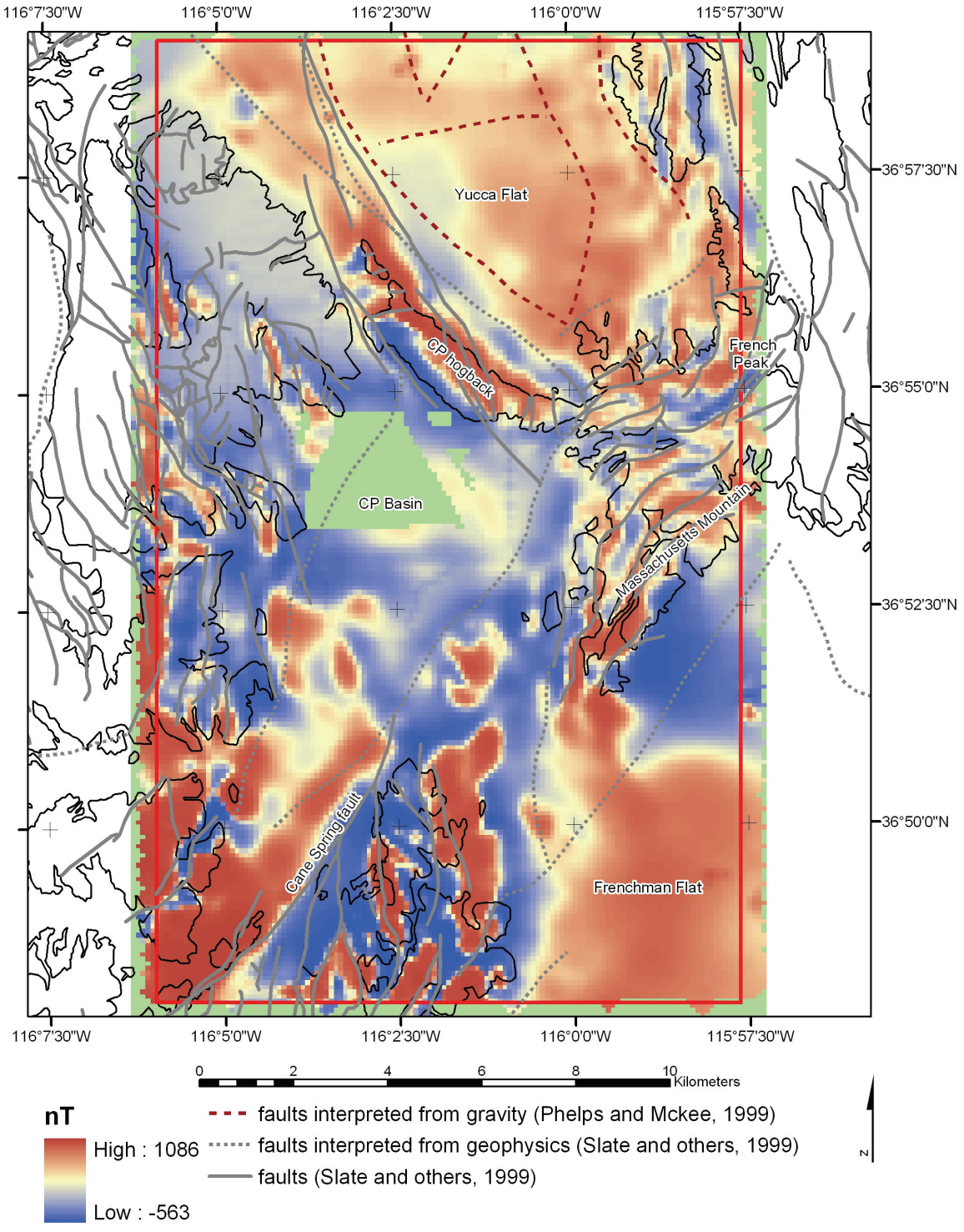

Figure 10a. Magnetic anomaly map for southern Yucca Flat and CP basin, shown with graticule and place names. Geology (black lines) generalized from Wahl and others (1997) and Slate and others (1999). Green patches are areas of missing data, and red bounding box is the boundary of the magnetic survey.

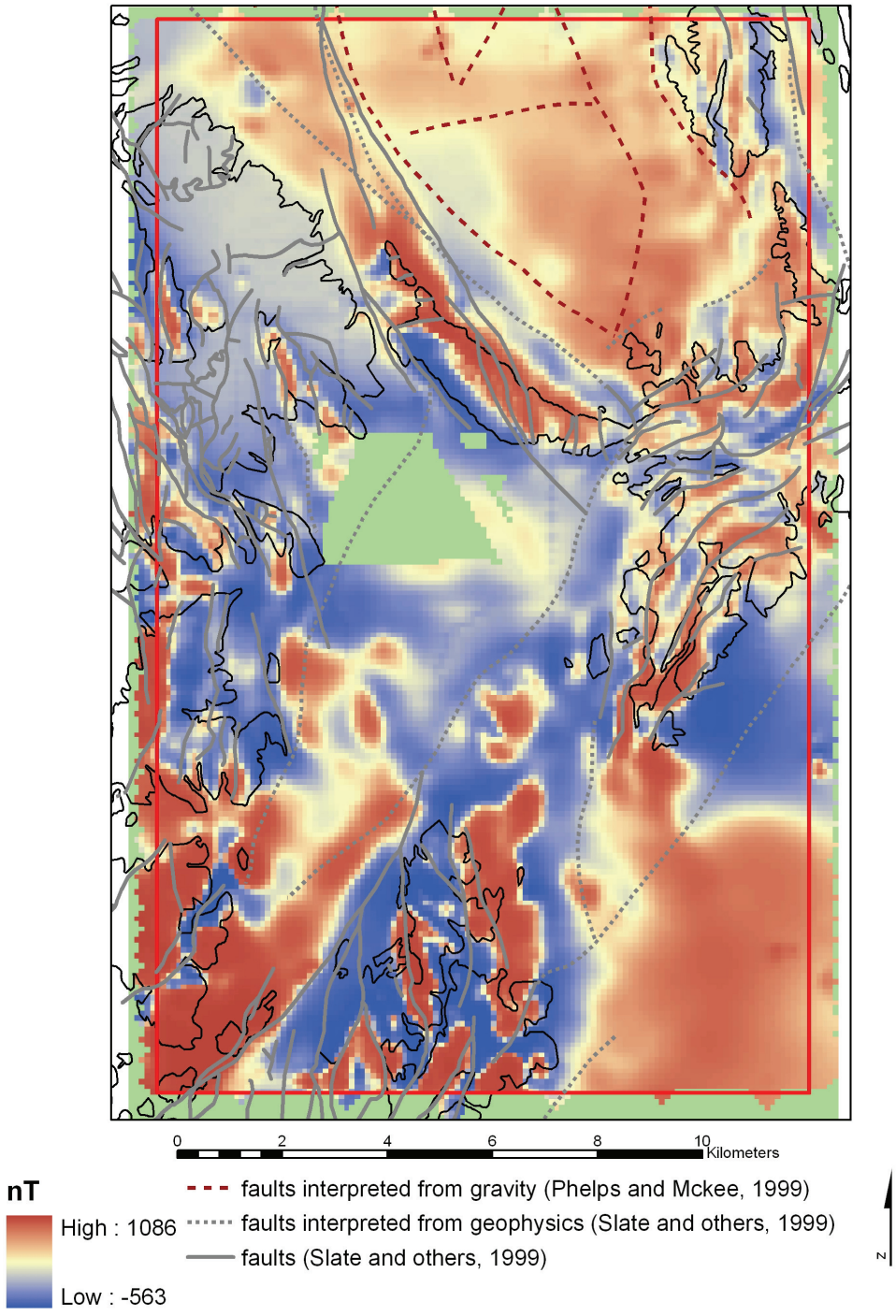

Figure 10b. Magnetic anomaly map for southern Yucca Flat and CP basin, with graticule and place names removed to show underlying patterns. Geology (black lines) generalized from Wahl and others (1997) and Slate and others (1999). Green patches are areas of missing data, and red bounding box is the boundary of the magnetic survey.

algorithm with a grid spacing of 100 m before delivery to the USGS (Geophex, Ltd, written communication) (fig. 10). The data from the survey are contained in appendix B.

The exposed magnetic Tertiary volcanics rocks in the study area are primarily tuffs of the Timber Mountain Group and the Wahmonie Tuff, with minor exposures of the Topopah Springs Tuff and older tuffs. Of the tuffs exposed in the area, only the lower part of the Timber Mountain Group, belonging to the Rainier Mesa Formation, is composed of tuffs that are reversely magnetized; the remainder of the tuffs are normally magnetized (Grauch and others, 1999; Kane and Bracken, 1983). In general, the remnant magnetization in the tuffs is aligned closely enough with the earth's magnetic field, within 25°, that the aeromagnetic anomaly can be used as a measure of total magnetization, and, therefore, can be used to characterize the magnetic rocks in the study area (Bath, 1968; Grauch, 1999).

Magnetic processing

The complex magnetic patterns shown in figure 10 indicate anomalies arise from a variety of sources lying at different depths. This superposition of anomalies can result in interpretational ambiguities. The principal goal of a magnetic study is to detect and quantify changes in magnetic properties at depth. Here we emphasize techniques to enhance particular anomaly characteristics, such as wavelength or trend. We discuss interpretations based on (1) reduction-to-pole to shift anomalies over their source rocks, (2) spectral analyses to separate magnetic data into anomaly components representing different source depths, and (3) horizontal gradient analysis to locate lateral changes in magnetization.

Reduction-to-pole

Total magnetization of rocks is the vector sum of two components; induced magnetization (which is proportional in magnitude and generally parallel to the Earth's ambient field) and remnant magnetization (which has a direction and intensity dependent on the origin and geologic history of the rock). It is assumed that the direction of remnant magnetization is parallel to, or nearly aligned with, the earth's magnetic field. This assumption is reasonable because most of the source rocks in the study areas are post-Cenozoic in age and, therefore, are likely to posses a remnant magnetization direction similar to that of the induced field. A reduction-to-pole filter was used to correct for the inherent asymmetry in the magnetic anomaly introduced by the angle by which the earth's magnetic field passes through the rock body. At earth's magnetic poles any induced magnetization is vertical, such that an anomaly over a symmetrical body is centered on the body. As the angle of incidence of earth's magnetic field decreases, as it does farther from the poles, the magnetic anomaly induced in the rock body becomes increasingly asymmetrical.

Spectral analysis

Match filtering (Phillips, 1997) separates the magnetic data into anomaly components reflecting sources at different depths. By transforming the data into the wavelength domain using a Fourier transform, characteristic wavelengths composing the magnetic field can be determined and related to source depth. A match filter was applied to the data to enhance the short and medium wavelength components that make up the magnetic anomaly field. These will be referred to as the anomaly components of shallow and medium-buried sources, respectively, to indicate that they emphasize shallow

(approximately < 250 m; fig. 11) and slightly deeper (approximately < 500 m; fig. 12) rocks. These components thus highlight the near-surface structure of the underlying volcanic tuffs.

Magnetic boundaries

The transformation of the magnetic field to magnetic potential (also called the pseudogravity transformation) generates the anomaly that occurs if the magnetization is replaced with an equivalent density distribution (Baranov, 1957). This allows for the application of horizontal gradient analysis, which helps define interpreted rock-unit boundaries on the basis of local curvature of the magnetic potential field (Blakely, 1995). The edges of rock bodies can be defined by the alignment of maximum horizontal gradient points. The maximum horizontal gradient is defined quantitatively for the filtered raster data sets using the method described by Blakely and Simpson (1986). This method identifies the points of maximum gradient in raster data sets, with particular emphasis on points that lie along linear gradients. In this paper the results (figs. 11a and 12a) are generalized to identify the raster grid cell in which the maximum gradient points occur rather than the exact location. The aeromagnetic anomaly map, with the maximum horizontal gradient points added, can be used to delineate areas with abrupt magnetization changes, indicating a lithologic related to deposition, erosion, or faulting of magnetic rocks within the study area. The boundaries of magnetic rocks appear as linear magnetic highs and lows, or as areas where the highs and lows are abruptly truncated. Considering these boundary locations in the context of geologic map information, the aeromagnetic anomaly can be used to characterize or map subsurface structures such as faults.

Results

Figures 11 and 12 illustrate the results of the shallow and medium source depths based on the match filtering process. In each figure, the map on the left (figs. 11a and 12a) shows the magnetic potential transformation, along with the points of maximum horizontal gradient and geology, while the map on the right (figs. 11b and 12b) removes some of this information so that the interpreted domains defined using the magnetic potential transformation can be seen more clearly. The points of maximum horizontal gradient locate near-steep boundaries of magnetic rocks. Large-amplitude, spatially persistent anomalies are likely to be caused by a single dominant source, and the location of the maximum horizontal gradient can be used as a guide to define its edges.

Figure 11 clearly shows the character of the outcropping magnetic rocks. Trends in the magnetic anomaly pattern follow mapped faulting, either coincident or aligned with the points of maximum gradient. This can be seen in Massachusetts Mountain where the faults trend north-northwest, near French Peak where the faults curve eastward, in the volcanic rock outcrops southeast of the Cane Spring fault (fig. 11b, domain C) and west of CP basin (fig. 11b, domain E) where the faults trend roughly north, and north of CP basin in the CP hogback (fig. 11b) where the faults trend southeast. Throughout the study area magnetic anomalies follow the trend of mapped faults exposed in outcrop. This correspondence can be used to extend these trends beneath the alluvium in the study area.

The most prominent feature in CP basin is the magnetic anomaly paralleling the Cane Spring fault. Northeast trending anomalies can be seen in the southwest corner of the study area (fig. 11b, domain A1 and domain A2). The anomalies match outcrops of

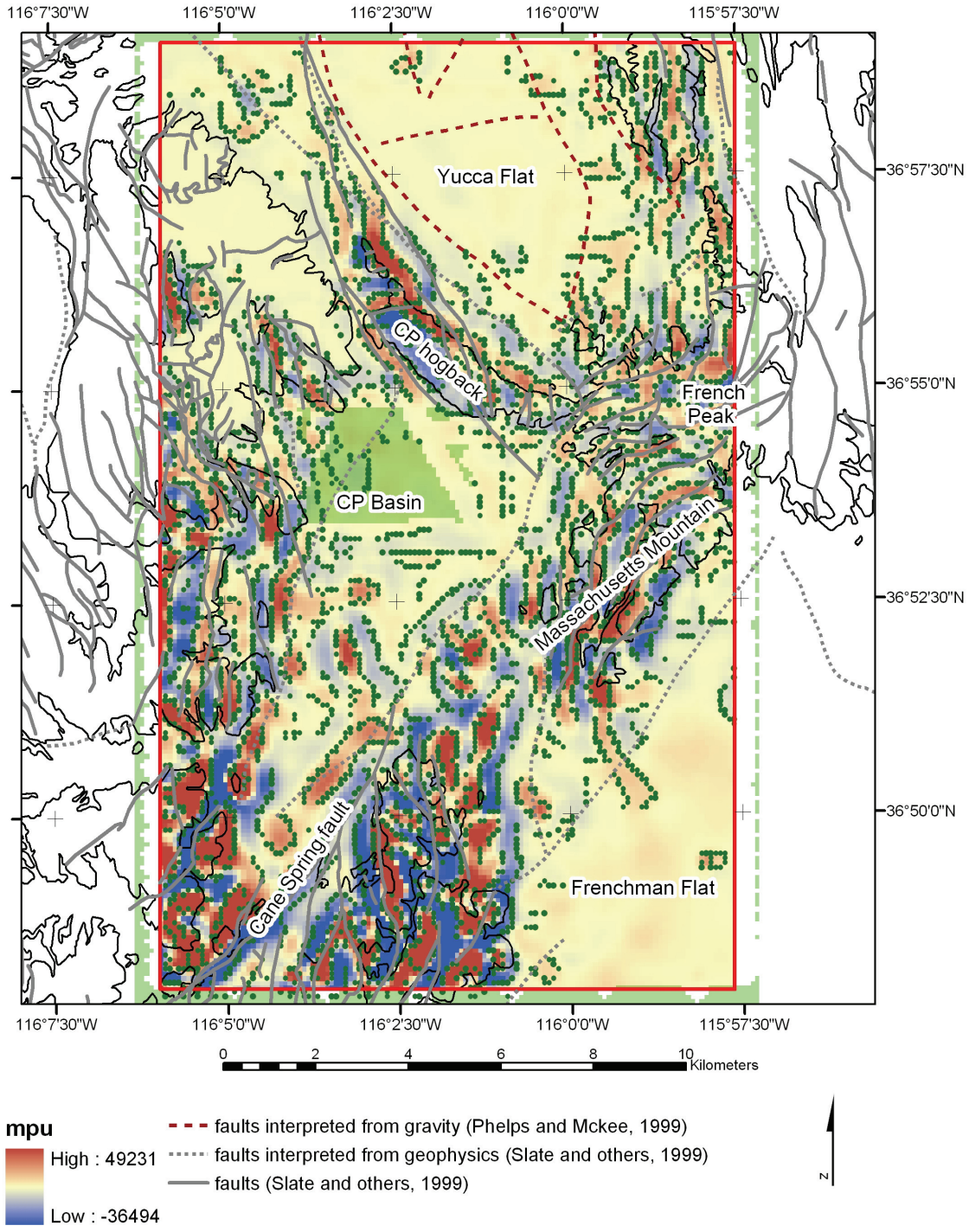

Figure 11a. Magnetic anomaly filtered to highlight shallow depth source rocks. The pseudogravity transformation is shown with the location of points of maximum horizontal gradient along linear trends (green circles). See figure 10a for explanation of figure symbols.

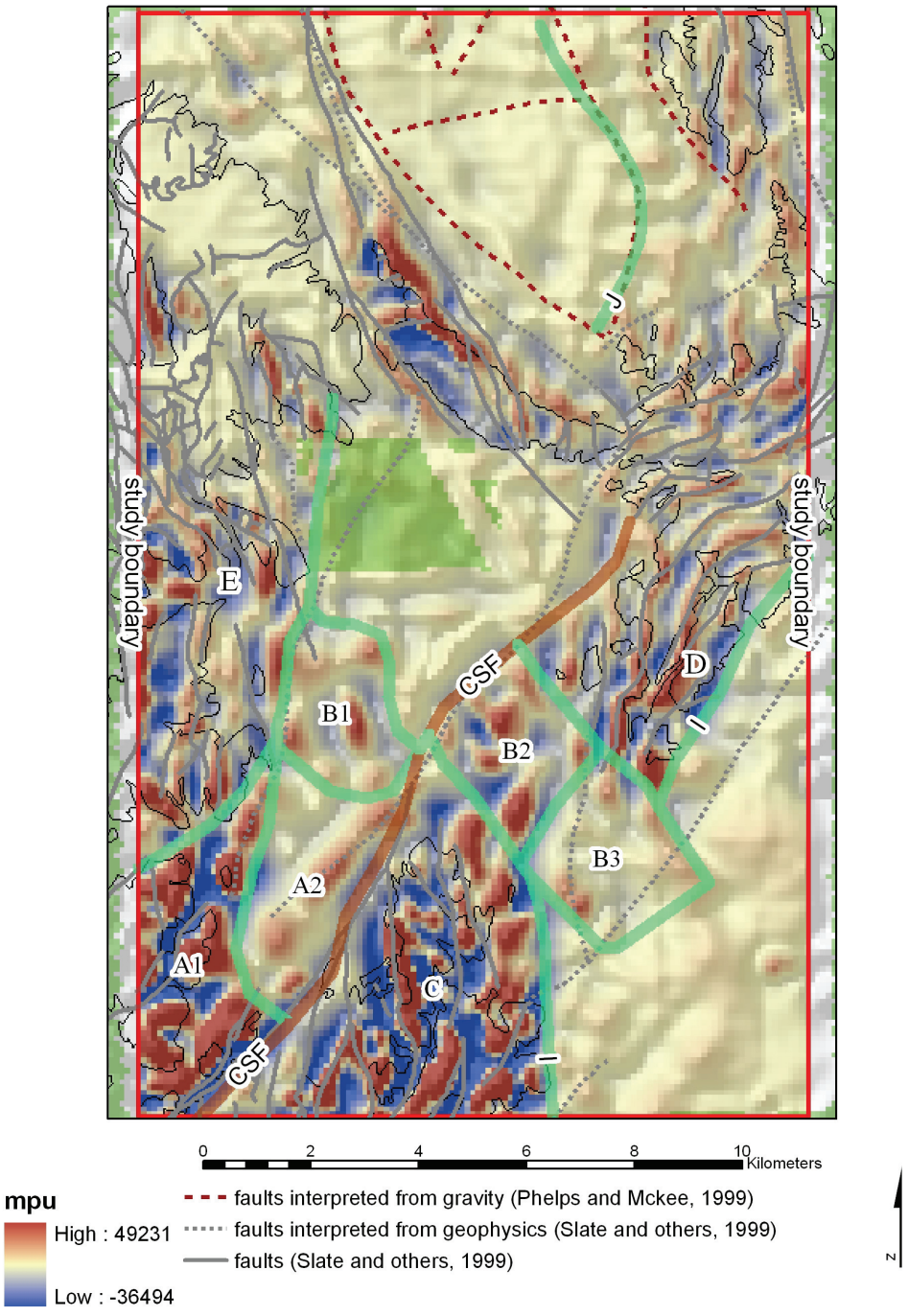

Figure 11b. Magnetic anomaly filtered to highlight shallow depth source rocks. The pseudo-gravity transformation is shown without location and maximum gradient information, and with shading, to highlight anomaly patterns. Thick green lines mark domain boundaries, thick red line shows the Cane Spring Fault, and labels (A1, A2, etc.) are domain boundaries discussed in the text. See figure 10a for explanation of figure symbols.

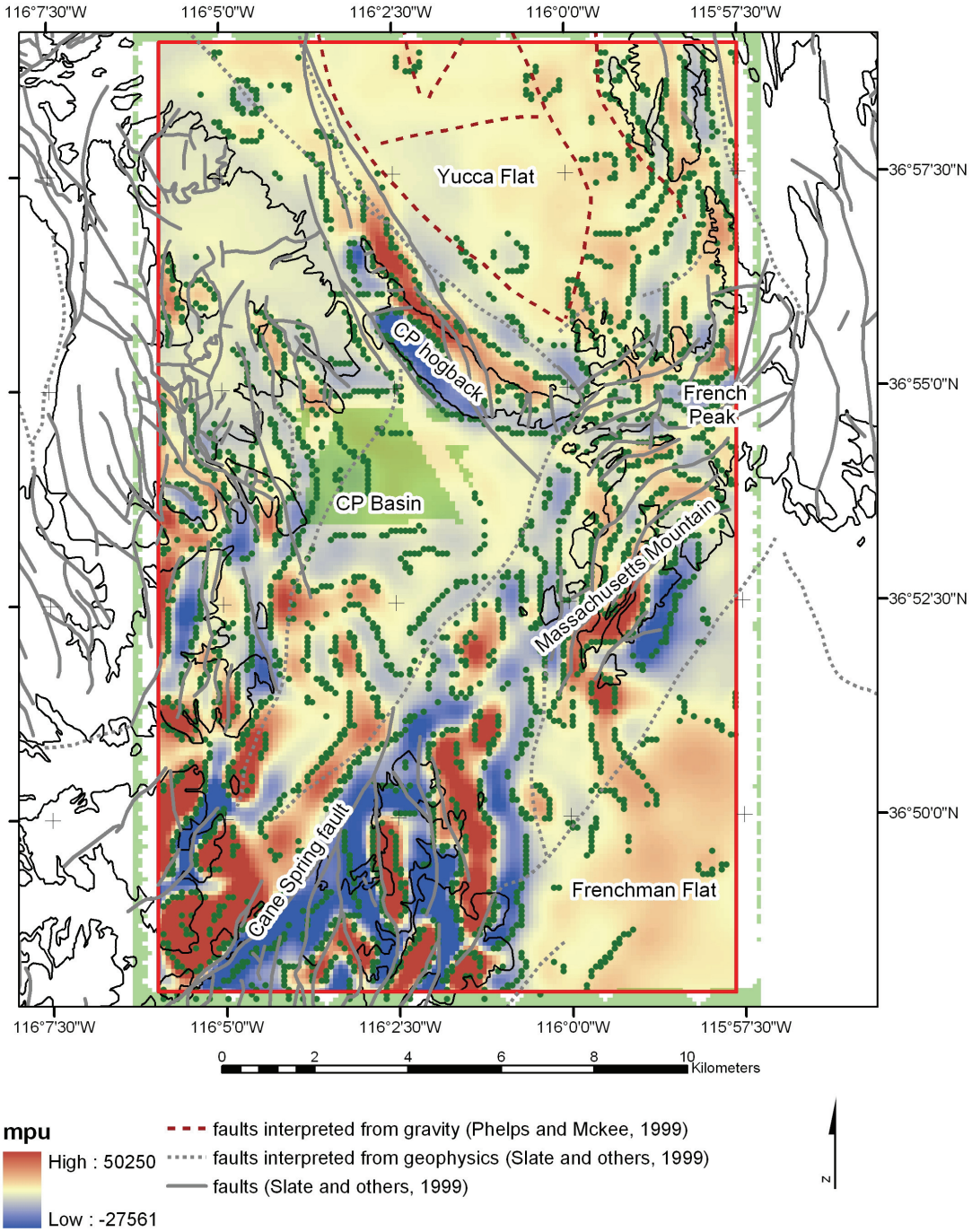

Figure 12a. Magnetic anomaly filtered to highlight intermediate depth source rocks. The pseudogravity transformation is shown with the location of points of maximum horizontal gradient along linear trends (green circles). See figure 10a for explanation of figure symbols.

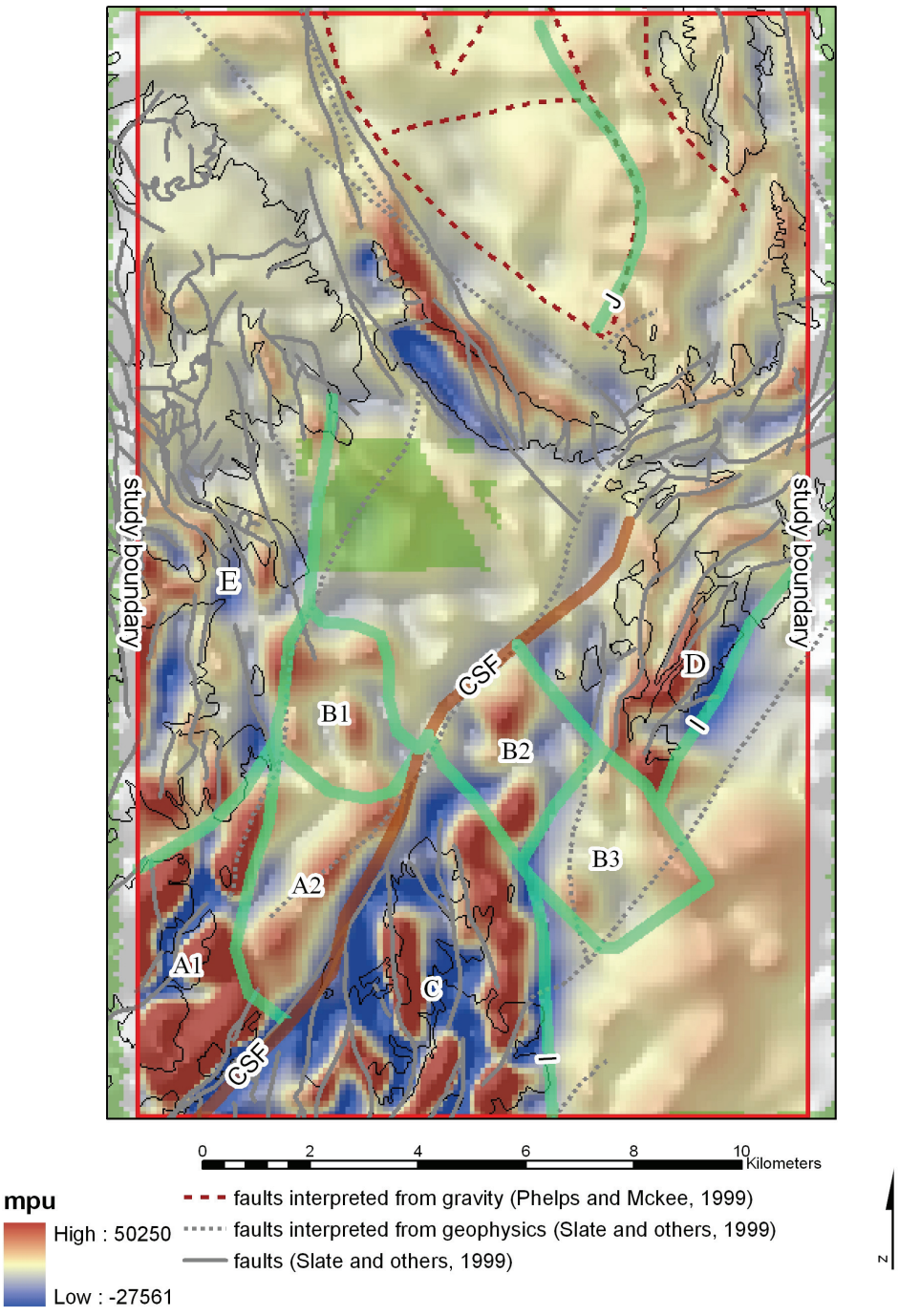

Figure 12b. Magnetic anomaly filtered to highlight intermediate depth source rocks. The pseudogravity transformation is shown without location and maximum gradient information, and with shading, to highlight anomaly patterns. Thick green lines mark domain boundaries, thick red line shows the Cane Spring Fault, and labels (A1, A2, etc.) are domain boundaries discussed in the text. See figure 10a for explanation of figure symbols.

volcanic rocks in domain A1 (figs. 11b and12b), and the strength of the anomalies decreases as the volcanic source rocks are buried beneath the alluvium in domain A2 (figs. 11b and 12b). This trend can be traced to Massachusetts Mountain as the magnetic anomalies south of the Cane Spring fault truncate against the Cane Spring fault boundary (fig. 11b, domain C and line CSF). As the mapped trace of the fault in southern CP basin becomes a geophysically-defined fault (Slate and others, 1999), the boundary is defined by the northern termination of prominent magnetic anomalies southwest of, and including, Massachusetts Mountain (fig. 11b, line CSF bounding domains B2 and D). West of this boundary in CP basin, the magnetic anomaly pattern is far less intense than that of the outcropping volcanic rocks in Massachusetts Mountain, indicating either a significant weakening in magnetism or more deeply buried magnetic source rocks. The existence of a basin and the presence of Timber Mountain and Paintbrush group volcanic rocks at depth in drill-holes WW4 and WW4A indicate deeper magnetic source rocks and imply that these rocks have been downed-dropped relative to Massachusetts Mountain.

The domain boundary interpreted as the Cane Spring fault is defined well by the magnetic anomaly and the gravity anomaly data, and it bounds the eastern side of CP basin. However, the basement ridge based on gravity inversion that separates CP basin from Frenchman Flat, noted earlier in this paper, does not correspond to the topographic ridge separating the two basins. The topographic ridge is displaced from basement ridge roughly two kilometers to the east.

On the east side of Massachusetts Mountain and extending south (fig. 11b, line I), the truncation of anomalies forms the boundary between the outcropping volcanic rocks in Massachusetts Mountain and the more subdued anomalies in Frenchman Flat. The change is abrupt rather than gradual, implying some component of normal slip on the fault separating the domains. Furthermore, the anomalies in Massachusetts Mountain appear to be offset to the east from the southern outcrop of volcanic rocks (fig. 11b, domains C and D). Secondary magnetic anomalies suggest a domain with weak northwest trending anomalies separating domains C and D (figure 11b, domains B2 and B3). These may correlate to the northwest-trending anomalies west of the Cane Spring fault (fig. 11b, domain B1). If these are piercing points it would imply approximately 3 km of left lateral movement along the Cane Spring fault, and would approximately line up the outcrops across the Cane Spring fault (northern part of domain A1 and northern part of domain C). The weaker anomalies in domain B3 relative to domain B2 suggest domain B3 has been down-dropped relative to domain B2.

In southern Yucca Flat the truncation of magnetic anomalies can be seen on the eastern side of the basin (fig. 11b, line J), approximately corresponding to the faults defined using the gravitational anomaly in Yucca Flat (Phelps and McKee, 1999).

The anomaly field of shallow sources (fig. 11) may reflect near-surface changes in the structure of the volcanic rocks. Minor faults can be distinguished from more significant structures by examining the continuity of anomalies from the shallow sources to that of anomalies related to medium depth sources (fig. 12). Areas of constant texture may define buried rock bodies at a constant depth.

The magnetic anomaly field from medium depth sources highlights the interpreted faults along both the west and east side of southern Yucca Flat, which supports the interpretations of Phelps and KcKee (1999). The differing intensity of distinct magnetic texture patches on the eastern side of Yucca Flat (fig. 12b, J) indicates volcanic units within the basin are down-dropped on the west. In general the faults inferred from the magnetic anomalies match well with those indicated by the gravity data (Phelps and

McKee, 1999). The magnetic data also indicate that the faults do not extend into Massachusetts Mountain or CP basin (figs. 11 and 12). The only faults that appear to be through-going from Yucca Flat into CP basin are the mapped faults that bound the CP hogback (Slate and others, 1999). The faults (figure 11b) follow the west side of Yucca Flat basin and trend south-southeast, bifurcating at CP hogback, with one strand trending southeast along the southern edge of CP hogback in CP basin, and terminate before reaching Massachusetts Mountain. This agrees with previous work (Carr, 1984; Hudson, 1997). In general, the north-trending faults present along the length of Yucca Flat bend, merge, and disappear before reaching CP hogback and Massachusetts Mountain or French Peak.

In the study area, the pattern of faults seen in outcrop is one of short faults that merge with other faults and curve, following general stress patterns; very few through-going faults are seen. It is reasonable to assume that faulting in the subsurface will follow this pattern. The Cane Spring fault appears to merge with faults in northwest Massachusetts Mountain, rather than cutting through to Yucca Flat basin. The fault pattern within northwestern CP basin is unfortunately obscured due to missing data (figs. 11a and 12a, green patch).

Hydrogeologic Implications

The work of Laczniak and others (1996) implies that pre-Tertiary strata form a structural/topographic high between Yucca Flat and CP basin which prohibits inter-basin groundwater flow through the Tertiary volcanic aquifers. Groundwater flow out of southern Yucca Flat, therefore, must do so through the regional aquifer. While many tectonic conceptual models for Cenozoic trans-tension in the region suggest that Yucca Flat, CP basin, and Frenchman Flat reside in separate, mechanically unconnected structural domains (e.g., Carr, 1984; Stewart, 1988; and O'Leary, 2000), it is unclear whether the interfaces between the hypothesized tectonic domains promote or hinder lateral groundwater flow through the regional aquifer. Furthermore, the strata composing the regional aquifer may be sufficiently thick to remain hydrologically connected even if significant amounts of vertical fault offset/unit juxtaposition have occurred (Cole and others, 1997; McKee, 1997). Another important factor in assessing the connectedness of the regional aquifer between basins, not considered in this study, is the configuration of pre-Tertiary units which have been deformed in several regional contractional events prior to the Cenozoic era.

Regional Aquifer Ground-water Flow Between Yucca Flat and CP Basin

Hydrological, geological, and the geophysical data presented by this study imply that the regional aquifer in Yucca Flat and CP basin could potentially be hydrologically disconnected. The water table in Cenozoic units in CP basin is elevated relative to that in southernmost Yucca Flat implying that there may be a barrier to lateral groundwater flow from southern Yucca Flat to CP basin (Winograd and Thordarson, 1975). The down-to-the-ENE normal faulting at CP hogback reported by Hudson (1997) and resolved by this geophysical study may be the feature producing offset that is significant enough to

impact the regional aquifer[2]. The geophysical data also imply that faults bounding the east side of Yucca Flat basin terminate north of CP hogback and Massachusetts Mountain, and, therefore, may not provide a pathway for or divert ground-water flow to CP basin. It is not possible to evaluate whether the regional aquifer in CP basin is connected to southern Yucca Flat using geochemical means at this time because no ground-water has been sampled from the regional aquifer in CP basin.

Regional Aquifer Ground-water Flow Between CP Basin and Frenchman Flat

Hydrological and geological data, and the geophysical data presented by this study suggest that the regional aquifer in CP basin and Frenchman Flat could potentially be hydrologically disconnected. The water table in Cenozoic units in CP basin is elevated relative to that in Frenchman Flat, which indicates that there may be a barrier to lateral groundwater flow from CP basin to Frenchman Flat (Winograd and Thordarson, 1975). Geologic maps by Poole, Elston, and Carr (1965) and Poole (1965) include several east-dipping faults along the western boundary of Frenchman Flat and several west-dipping faults along the eastern boundary of CP basin. The magnetic data presented here indicate that offset along the Cane Spring fault continues up to Massachusetts Mountain in northern CP basin and that offset along west-bounding faults of Frenchman Flat basin continues to the northernmost portion of the basin. The cumulative offset along this structurally complex area may be enough to juxtapose the regional aquifer against impermeable lithologies and impede ground-water flow through the regional aquifer. It is not possible to evaluate whether the regional aquifer in CP basin is disconnected from Frenchman Flat using geochemical means at this time because no ground-water has been sampled from the regional aquifer in CP basin.

Regional Aquifer Ground-water Flow Between Yucca Flat and Frenchman Flat

Geochemical data suggest that there may be a hydrologic connection between the regional aquifer in southwestern Yucca Flat and Frenchman Flat. However, geologic data and the geophysical data presented by this study delineate the presence of numerous structures which could potentially hydrologically disconnect the regional aquifer in southwestern Yucca Flat and Frenchman Flat. The major cation, major anion, Sr, Cl^-, $^{87}Sr/^{86}Sr$, δD, and $\delta^{18}O$ composition of ground-water from the regional aquifer in southwestern Yucca Flat (wells WWC-1 and WWC) is very similar to that from the regional aquifer in northern Frenchman Flat (well 5-3 #2, Hershey and others, 2005). Alternatively, the composition of ground-water from the regional aquifer in southeastern Yucca Flat (wells ER6-1 #2 and ER6-1) has a distinctly different chemical composition to that from the regional aquifer in northwestern Frenchman Flat (well 5-3 #2, Hershey and others, 2005) implying that there may not be a hydrologic connection between southeastern Yucca Flat and northwestern Frenchman Flat. Geologic maps by Poole, Elston, and Carr (1965), Hinrichs and McKay (1965), and Hudson (1997) include a

[2] The most likely barriers to lateral groundwater flow in this region are late Cenozoic transtension-related faults that may juxtapose the regional aquifer against impermeable lithologies such as Precambrian to Cambrian siliciclastic units, Tertiary zeolitized tuff, or the Rocks of Pavits Spring (Prothro and Drellack, 1997).

complex zone of brittle deformation in the vicinity of French Peak. The magnetic data presented here indicate that offset along the Cane Spring fault continues to the northernmost portion of CP basin and that offset along west-bounding faults of Frenchman Flat basin continues to the northernmost portion of the basin. The cumulative offset along this structurally complex area may be enough to juxtapose the regional aquifer against impermeable lithologies and impede ground-water flow through the regional aquifer.

Conclusions

The density and gravity modeling indicates that CP basin is a shallow, oval-shaped basin which trends north-northeast and contains ~800 m of basin-filling volcaniclastic and sediment at its deepest point. The deepest part of the basin is in the northeast while the southern part of the basin is very shallow. CP basin is separated from the deeper Frenchman Flat basin by a subsurface ridge that may represent a Tertiary-aged erosion surface at the top of the Paleozoic strata which cuts deeper into the Paleozoic strata toward the eastern edge of Massachusetts Mountain. The magnetic modeling indicates that the Cane Spring fault bounds the CP basin domain on the east. The Cane Spring fault appears to merge with faults in northwest Massachusetts Mountain, rather than cut through to Yucca Flat basin. A weaker magnetic anomaly pattern and drill-hole data in northeast CP basin imply that the basin is downed-dropped relative to Massachusetts Mountain. An abrupt change in magnetic anomalies on the east side of Massachusetts Mountain suggests some component of normal slip on the Cane Spring fault. Secondary magnetic anomalies suggest a domain with weak northwest trending anomalies separating subdomains in CP basin and in the saddle south of Massachusetts Mountain and between CP basin and Frenchman Flat. Potential offset patterns along these faults imply approximately 3 km of left lateral movement along the Cane Spring fault.

The magnetic anomaly field from medium depth sources highlights the interpreted faults along both the west and east side of southern Yucca Flat, which supports the interpretations of Phelps and KcKee (1999). Variations in magnetic intensities indicate volcanic units within Yucca flat basin are down-dropped on the west. In southern Yucca Flat the truncation of magnetic anomalies can be seen on the eastern side of the basin. The magnetic data indicate that the only faults that appear to be through-going from Yucca Flat into either Frenchman Flat or CP basin are the faults that bound the CP hogback. This agrees with previous work (Carr, 1984; Hudson, 1997). In general, the north-trending faults present along the length of Yucca Flat bend, merge, and disappear before reaching CP hogback and Massachusetts Mountain or French Peak.

Acknowledgments

The authors would like to thank the U.S. Department of Energy for funding this research. This work benefited greatly from many helpful reviews and discussions, in particular from D. Sweetkind, R. Blakely, G. Pawloski, P. Kassemeyer, S. Drellack, L. Prothro, D. O'Leary, A. Cogbill, and T. Hildenbrand. The authors would like to thank the reviewers for their time and effort.

References Cited

Baranov, V., 1957, A new method for interpretation of aeromagnetic maps: pseudogravimetric anomalies, Geophysics, v.2, no. 2, pp. 59-383.

Bath, G.D., 1968, Aeromagnetic anomalies related to remanent magnetism in volcanic rock, Nevada Test Site: Geological Society of America Memoir 110, p. 135-146.

Blakely, R.J., 1995, Potential Theory in Gravity and Magnetic Applications: Cambridge University Press, New York, NY, 441 p.

Blakely, R.J., and Simpson, R.W., 1986, Approximating edges of source bodies from magnetic or gravity anomalies: Geophysics, v.51, p. 1494-1496

Burkhard, N.R., 1989, Physical properties in LLNL Yucca Flat Areas: the rock pile concept: 5th Symposium of the Containment of Underground Nuclear Detonations, Mission Research in Santa Barbara, California, September 19-21, 1989.

Carr, W.J., 1984, Regional structural setting of Yucca Mountain, south-western Nevada, and late Cenozoic rates of tectonic activity in part of the Southwestern Basin, Nevada and California: U.S. Geological Survey Open-File Report 84-854, 109 p.

Cole, J.C., Harris, A.G., and Wahl, R.R., 1997, Sub-crop geologic map of pre-Tertiary rocks in the Yucca Flat and northern Frenchman Flat areas, Nevada Test Site, southern Nevada: U.S. Geological Survey Open-File Report 97-678, 24 p.

Dobrin, M.B., and Savit, C.H., 1988, Introduction to Geophysical Prospecting, fourth edition: Mcgraw-Hill, New York, 867 p.

Ferguson, J. F., Felch, R. N., Aiken, C. L.V., Oldow, J. S., and Dockery, Holly, 1988, Models of the bouguer gravity and geologic structure at Yucca Flat, Nevada: Geophysics, v. 53, n. 2, p. 231.

Grauch, V.J.S., Sawyer, D.A., Fridrich, C.J., and Hudson, M.R., 1999, Geophysical framework of the southwestern Nevada volcanic field and hydrogeologic implications: U.S. Geological Survey Professional Paper 1608, 40 p.

Healey, D.L., 1968, Application of gravity data to geologic problems at Nevada Test Site: Geological Society of America Memoir 110, p. 147-156.

Healey, D.L., Clutsom, F.G., and Glover, D.A., 1984, Borehole gravity meter surveys in drill holes USW G-3, UE-25p#1, and UE-25c#1, Yucca Mountain area, Nevada: U.S. Geological Survey Open-File Report 84-672, 16 p.

Healey, D.L., Clutsom, F.G., and Glover, D.A., 1986, Borehole gravity meter surveys in drill hole USW G-4, Yucca Mountain Area, Nye County, Nevada: U.S. Geological Survey Open-File Report 86-205, 18 p.

Hershey, R.L., Thomas, J.M., Rose, T.P., Paces, J.B., Farnham, I.M., and Benedict, F.C., Jr., 2005, Evaluation of groundwater movement in the Frenchman Flat CAU using geochemical and isotopic analysis: Desert Research Institute, 45207, 65 p.

Hildenbrand, T.G., Langenheim, V.E., Mankinen, E.A., and McKee, E.H., 1999, Inversion of gravity data to define the pre-Tertiary surface and regional structures possibly influencing ground-water flow in the Pahute Mesa-Oasis Valley Region, Nye County, Nevada: U.S. Geological Survey Open-File Report 99-49, 29 p.

Hinrichs, Neal E., and McKay, Edward J., 1965, Geologic map of the Plutonium Valley Quadrangle, Nye and Lincoln Counties, Nevada: U.S. Geological Survey, scale 1:24,000.

Hudson, M.R., 1997, Structural geology of the French Peak accommodation zone, Nevada Test Site, southwestern Nevada: U.S. Geological Survey Open-File Report 97-56, 26 p.

International Union of Geodesy and Geophysics, 1971, Geodetic Reference System 1967: International Association of Geodesy Special Publication 3, 116 p.

Jachens, R.C., and Moring, B.C., 1990, Maps of the thickness of Cenozoic deposits and the isostatic residual gravity over basement for Nevada: U.S. Geological Survey Open-File Report 90-404, 15 p., 2 plates, scale 1:1,000,000.

Jachens, R.C., and Griscom, Andrew, 1985, An isostatic residual gravity map of California -- A residual map for interpretation of anomalies from intracrustal sources; in Hinze, W.J. ed., The utility of regional gravity and magnetic anomaly maps: Tulsa, Okla., Society of Exploration Geophysics, p. 347-360.

Kane, M.F., and Bracken, R.E., 1986, Aeromagnetic map of Yucca Mountain and surrounding regions, southwest Nevada: U.S. Geological Survey Open-File Report 83-616, p.

Kososki, Bruce A., Robbins, Stephen L., and Schmoker, James W., 1987, Principal facts for borehole gravity stations in test well Ue19z, exploratory drill hole PM-1, and water well 5a, Nevada Test Site, Nye County, Nevada: U.S. Geological Survey Open-File Report 78-983, 16 p.

Laczniak, R.J., Cole, J.C., Sawyer, D.A., and Trudeau, D.A., 1996, Summary of hydrogeologic controls on ground-water flow at the Nevada Test Site, Nye County, Nevada: U.S. Geological Survey Water-Resources Investigations Report 96-4109, 59 p.

McKee, E.H., 1997, Evaluation of geologic structure guiding ground water flow south and west of Frenchman Flat, Nevada Test Site: U.S. Geological Survey Open-File Report 97-734, 26 p.

Morelli, C. (Ed.), 1974, The International Gravity Standardization Net, 1971: International Association of Geodesy Special Publication no. 4, 194 p.

Murray, D.A., Ridgway, K.D., Stamatakos, J.A., and Gray, M.B., 2001, Stratigraphy and tectonic implications of upper Oligocene and lower Miocene strata in the Yucca Mountain Area: Geological Society of America Abstracts with Programs, v. 33, no. 6, p. 79.

O'Leary, D.W., 2000, Tectonic significance of the Rock Valley fault zone, Nevada Test Site, in, Whitney, J.W. and Keefer, W.R., eds., Geological and geophysical characterization studies of Yucca Mountain, Nevada: U. S. Geological Survey Digital Data Series, Report: DDS-0058, 13 pp.

Phelps, G.A., Langenheim, V.E., and Jachens, R.C., 1999, Thickness of Cenozoic deposits of Yucca Flat inferred from gravity data, Nevada Test Site, Nevada: U.S. Geological Survey Open-File Report 99-310, 32 p.

Phelps, G.A., and McKee, E.H., 1999, High-angle faults in the basement of Yucca Flat, Nevada test Site, Nevada, based on the analysis of a constrained gravity inversion surface: U.S. Geological Survey Open-File Report 99-383, 10 p.

Phelps, G.A., and Graham, S.E., 2002, Preliminary gravity inversion model of Frenchman Flat basin, Nevada Test Site, Nevada: U.S. Geological Survey Open-File Report 02-363, 23 p.

Phillips, J., 1997, Potential-Field Geophysical Software for the PC, version 2.2: U.S. Geological Survey Open-File Report 97-725, http://pubs.usgs.gov/of/1997/ofr-97-0725/ (date of most recent access: December 15, 2005).

Ponce, D.A., 1997, Gravity data of Nevada: U.S. Geological Survey Digital Data Series DDS-42, CD-ROM.

Plouff, D., 1977, Preliminary documentation for a FORTRAN program to compute gravity terrain corrections based on topography digitized on a geographic grid: U.S. Geological Survey Open-File Report 77-535, 45 p.

Poole, F.G., 1965, Geologic map of the Frenchman Flat quadrangle, Nye, Lincoln, and Clark counties, Nevada: U.S. Geological Survey Geologic Quadrangle Map GQ-465.

Poole, F.G., Elston, D.P., and Carr, W.J., 1965, Geologic map of the Cane Spring quadrangle, Nye County, Nevada: U.S. Geological Survey Geologic Quadrangle Map GQ-455.

Prothro, L.B., and Drellack, S.L., Jr., 1997, Review and reconnaissance of the hydrogeology of Tertiary sedimentary rocks in the vicinity of Frenchman Flat, Nevada Test Site: Technical Report DOE/NV/11718-155, Bechtel Nevada, Las Vegas, NV, 63 p.

Raines, G.L., Connors, K.A., Moyer, L.A., and Miller, R.J., 2003, Spatial digital database for the geologic map of Nevada: U.S. Geological Survey Open-file report 03-066.

Robbins, S.L., Schmoker, J. W., and Hester, T.C., 1982, Principal facts and density estimates for borehole gravity stations in exploratory wells Ue4ah, Ue7j, Ue1h, Ue1q, Ue2co, and USW-H1 at the Nevada Test Site, Nye County, Nevada,: U.S. Geological Survey Open-File Report 82-277, 33 p.

Robbins, S.L., and Clutsom, F.G., 1983, Principal facts and density estimates for borehole gravity stations in exploratory wells Ue7h, Ue4al, and Ue11a at the Nevada Test Site, Nye County, Nevada,: U.S. Geological Survey Open-File Report 83-244, 20 p.

Schmoker, James W., and Kososki, Bruce A., 1978, Principal facts for borehole gravity stations in test wells Ue10j, Ue7ns, and Ue5n, Nevada Test Site, Nye County, Nevada: U.S. Geological Survey Open-File Report 78-212, 5 p.

Slate, J.L., Berry, M.E., Rowley, P.D., Fridrich, C.J., Morgan, K.S., Workman, J.B., Young, O.D, Dixon, G.L., Williams, V.S., McKee, E.H., Ponce, D.A., Hildenbrand, T.G., Swadley, W, 1999, Digital Geologic Map of the Nevada Test Site and Vicinity, Nye, Lincoln, and Clark Counties, Nevada and Inyo County, California, Revision 4: U.S. Geological Survey, Open-File Report 99-554-A.

Stewart, J.H., 1988, Tectonics of the Walker Lane belt, western Great Basin-Mesozoic and Cenozoic deformation in a zone of shear, in, Ernst, W.G., ed., Metamorphism and crustal evolution of the western United States, volume 7: Prentice Hall, p. 684-713.

Tukey, J.W., 1977, Exploratory Data Analysis: Addison-Wesley, Reading, Massachusetts, 688 p.

Wahl, R.R., Sawyer, D.A., Carr, M.D., Minor, S.M., Cole, J.C., Swadley, W.C., Laczniak, R.J., Warren, R.G., Green, K.S., and Engle, C.M., 1997, Digital geologic map database of the Nevada Test Site area, Nevada: U.S. Geological Survey Open-File Report 97-140, scale 1:100,000, 47 p.

Winograd, I.J., and Thordarson, W., 1975, Hydrogeologic and hydrochemical framework, south-central Great Basin, Nevada-California, with special reference to the Nevada Test Site: U.S. Geological Survey Professional Paper 712-C, 125 p.

Workman and others, 2002, Geologic map of the Death Valley ground-water model area, Nevada and California: U.S. Geological Survey Miscellaneous Field Studies Map 2381-A.